Disentangling future effects of climate change and forest disturbance on vegetation composition and land-surface properties of the boreal forest

Lucia S. Layritz[1], Konstantin Gregor[1], Andreas Krause[1], Stefan Kruse[2], Benjamin F. Meyer[1], Tom A. M. Pugh[3, 4, 5], and Anja Rammig [1]

[1]Land Surface–Atmosphere Interactions, TUM School of Life Sciences, Technical University of Munich, Freising, Germany
[2]Alfred Wegener Institute Helmholtz Centre for Polar and Marine Research, 14473 Potsdam, Germany
[3]School of Geography, Earth and Environmental Sciences, University of Birmingham, Birmingham, B15 2TT, United Kingdom
[4]Birmingham Institute of Forest Research, University of Birmingham, Birmingham, B15 2TT, United Kingdom
[5]Department of Physical Geography and Ecosystem Science, Lund University, Lund, Sweden

Correspondence: Lucia S. Layritz (lucia.layritz@tum.de)

Abstract. Forest disturbances can cause shifts in boreal vegetation cover from predominantly evergreen to deciduous trees or non-forest dominance. This, in turn, impacts land surface properties and, potentially, regional climate. Accurately considering such shifts in future projections of vegetation dynamics under climate change is crucial but hindered e.g. uncertainties in future

5   disturbance regimes. In this study, we investigate how sensitive future projections of boreal forest dynamics are to additional changes in disturbance regimes. We use the dynamic vegetation model LPJ-GUESS to investigate and disentangle the impacts of climate change and intensifying disturbance regimes in future projections of boreal vegetation cover as well as changes in land surface properties such as albedo and evapotranspiration. Our simulations find that warming alone drives shifts towards more densely forested landscapes, and more intense disturbances reduce tree cover in favor of shrubs and grasses, while

10   the interaction between climate and disturbances leads to an expansion of deciduous trees. Our results additionally indicate that warming decreases albedo and increases evapotranspiration, while more intense disturbances have the opposite effect, potentially offsetting climate impacts. Warming and disturbances are thus comparably important agents of change in boreal forests. Our findings highlight future disturbance regimes as a key source of model uncertainty and underscore the necessity of accounting for disturbances-induced effects on vegetation composition and land surface-atmosphere feedback.

1   Introduction

15   Climate change induces widespread changes in ecosystem state and functions (McDowell et al. (2020); Allen et al. (2010)). Next to changing mean conditions, climate change is expected to lead to an increase in extreme climatic events in many regions (Calvin et al. (2023); Field (2012); Rahmstorf and Coumou (2011)). On the ecosystem level, this alters regimes of ecosystem disturbances such as fire, windthrow, or biotic agents (McDowell et al. (2020); Seidl et al. (2017); Reichstein et al. (2013)).

20   Disturbances may lead to widespread tree mortality and loss of forest cover. While they are inherent elements of many forest ecosystems, changes in disturbance regimes (that is, changes in their frequency, intensity, or size) can have profound impacts, especially in systems already subjected to environmental pressure (Pugh et al. (2019a); Allen et al. (2010)). Understanding the impact of disturbances is therefore crucial for reliably projecting the future development of forest ecosystems under climate change.

25   The boreal forest, or Taiga, is the second largest terrestrial biome in both area and carbon mass (Pan et al. (2011); Malhi et al. (1999)), spanning the Northern Hemisphere in a circumpolar band between approximately 50^oN and 70^oN. (Pfadenhauer and Klötzli (2020)). Its characteristic vegetation are conifer forests, dominated by various species of *Abies*, *Picea*, and *Pinus* in North America and Western Eurasia and by *Larix* in Siberia (Pfadenhauer and Klötzli (2020)). In the boreal forest, disturbances are an integral part of ecosystem dynamics, and tree species are thus adapted and resilient to historical disturbance regimes

30   (Pfadenhauer and Klötzli (2020); Ilisson and Chen (2009); Johnstone et al. (2010)). However, evidence from both paleoecology (Peros et al. (2008); Edwards et al. (2005)) and recent field surveys (Baltzer et al. (2021); Mack et al. (2021); Johnstone et al. (2010); Brice et al. (2020)) suggest that changing disturbance regimes can disrupt existing successional cycles and induce reorganization of the complete ecosystem. In many places, evergreen needleleaf trees fail to regenerate after disturbance and transitions to broadleaf summergreen forests or non-forest ecosystems are reported (Baltzer et al. (2021); Mack et al. (2021)).

35   Boreal forests influence regional and global climate (Bonan (2008)). Aside from being a carbon sink, vegetation composition influences surface properties such as albedo or evapotranspiration. Swann et al. (2010); Liu et al. (2019); Rogers et al. (2013); Bonan (2008); Chapin et al. (2005)). Shifts in vegetation composition can, therefore, result in significant alterations to the carbon, water, and energy balance of the region (Mack et al. (2021); Boisier et al. (2013); Zhang et al. (2013); Alexander et al. (2012); Swann et al. (2010); Bonan (2008)). Consequently, their role and accurate representation in projections of future

40   vegetation and climate dynamics is important.

Several studies have tackled part of this question: Kim et al. (2024); Wang et al. (2020) and Sulla-Menashe et al. (2018) have aimed to quantify the disturbance effect from observations. However, this remains incomplete as disturbed sites are also subject to background climate change, and the disturbance effect can therefore not be isolated. Additionally, observational time series of forest dynamics, especially large-scale assessments from remote sensing, are still relatively short ($\sim$ 30 years) compared

45   to the multidecadal to centennial time scales of forest succession. Therefore, it remains difficult to pinpoint if the observed changes will be permanent or transient in nature.

Process-based vegetation models are a prime research tool to complement observational findings in these regards, as they allow for the factorial simulation of different drivers over longer time periods. Zhang et al. (2020); Warlind et al. (2014); Zhang et al. (2013); Warszawski et al. (2013), and Wolf et al. (2008) explored the impact of future climate change on boreal forest

50   dynamics and land surface properties with dynamic vegetation models (DVMs) without considering changes in disturbance regimes. Rogers et al. (2013) investigated the impact of changing disturbance regimes on land surface properties and climate but did not consider climate change effects on vegetation. Hansen et al. (2021), Brice et al. (2020), and Mekonnen et al. (2019) explored the interplay of climate change and disturbance regimes for parts of Alaska and Canada over the 21st century. Additionally, none of these studies explored long-term effects and regeneration after disturbance. To our knowledge, there

55 so far exist no modeling studies that systematically investigated the immediate and long-term (centennial) impacts of both changing disturbance regimes, climate change, and their interaction on evergreen boreal forest dynamics across the biome for different climate futures.

In this study, we use the DVM LPJ-GUESS (Smith et al. (2001, 2014)) to fill this gap. LPJ-GUESS includes a process-based representation of plant physiology (photosynthesis, respiration, and evapotranspiration) and resolves vegetation structure on

60 the level of individual tree cohorts, organized in multiple patches across the landscape. This allows for the simulation of disturbances, mortality, and establishment in a way well suited to study disturbance regimes and post-disturbance regeneration. We perform factorial simulation experiments of both different climate scenarios and external disturbance regimes to disentangle their respective future roles in vegetation dynamics of high-latitudinal forests.

We address the following research questions: (1) What is the impact of climate change, changing disturbance regimes, and

65 their interactive effect on boreal vegetation composition? (2) How do changes in vegetation influence climate-relevant biogeo-physical land surface properties, namely albedo and evapotranspiration? (3) Are disturbance-induced changes permanent, or is vegetation able to regenerate once disturbance pressure is again lifted?

2 Methods

2.1 Vegetation modeling

70 #### 2.1.1 General LPJ-GUESS Model Description

We work with version 4.1 of the well-established dynamic vegetation model LPJ-GUESS (Smith et al. (2001, 2014); Nord et al. (2021)), driven by gridded temperature, precipitation, and downwelling shortwave radiation, as well as global CO_2 concentrations and soil properties. We here use a version parametrized for Arctic vegetation as summarized in Table A2, which has been validated in previous studies (e.g. Zhang et al. (2013); Miller and Smith (2012); Wolf et al. (2008).

75 Plant physiological processes follow the approach of LPJ-DGVM (Sitch et al. (2003)). As the focus of this study is on vegetation dynamics, we here briefly sketch out the main processes - described in detail by Smith et al. (2001) and Smith et al. (2014) - followed by a detailed description of population dynamics and disturbances. CO_2 and water fluxes are calculated by a coupled photosynthesis and stomatal conductance scheme based on the approach of BIOME3 (Haxeltine and Prentice (1996)). Each simulation year, the NPP accrued by an average individual plant is allocated to leaves, fine roots, and, for woody

80 plants, sapwood, following a set of prescribed allometric relationships (Sitch et al. (2003)). Litter from phenological turnover, mortality, and disturbances enters the soil decomposition cycle. For details on soil processes, including C-N dynamics and soil hydrology, refer to Smith et al. (2014); Sitch et al. (2003) and Gerten et al. (2004).

2.1.2 Population and disturbance dynamics in LPJ-GUESS

LPJ-GUESS employs a hierarchical model structure that allows for a detailed representation of population dynamics such as

85 recruitment, competition and disturbance. Within each grid cell of climate data, multiple patches are simulated (25 patches

are used in this study). Patches can be thought of as a random, independent sample of the gridcell, the model thus outputs the average across all patches in a grid cell. Vegetation dynamics within each patch emerge from growth and competition for light, space, and soil resources among woody plant cohorts and a herbaceous understory. Plants within a patch are represented by different age cohorts of a number of plant functional types (PFTs) described by properties such as growth form, phenology,

90 photosynthetic pathway (C3 or C4), and bioclimatic limits (see Table A1 for the PFT parametrization used in this study). Each age cohort includes multiple individuals of that PFT assumed to all have identical properties ('cohort mode'). Establishment and mortality are represented as stochastic processes on the cohort level (see Appendix A1 for a detailed description).

in LPJ-GUESS, disturbances occur on the patch level with a yearly disturbance probability p_D. If a patch experiences a disturbance, aboveground vegetation is converted to coarse woody debris and slowly decomposes over time. The patch

95 structure here emulates heterogeneity in the landscape and accounts for the fact that disturbances are not necessarily stand-replacing on the landscape scale. We opted for this standardized implementation of disturbances to reduce degrees of freedom in our experiments and be able to focus on downstream impacts.

2.2 Input Data

We run LPJ-GUESS with daily simulated climate from the Inter-Sectoral Impact Model Intercomparison Project (ISIMIP)

100 repository on a 0.5° x 0.5° resolution (Lange and Büchner (2021)). From within the ISIMIP ensemble, data of the MRI-ESM2.0 Earth system model was chosen, as its response best represents the ensemble average. We also use corresponding yearly atmospheric CO_2 concentration data from ISIMIP. Figure 1a shows the CO_2 concentration, and Fig. A1 the climate data used. We use soil data from the Harmonized World Soil Database, aggregated to the resolution of the climate data (FAO and IIASA (2023)). The model assumes yearly nitrogen deposition of 750 gha^{-1} (Tian et al. (2018)).

105 2.3 Modeling Protocol

We ran LPJ-GUESS with all scenarios available from the ISIMIP (SSP1-RCP2.6, SSP3-RCP7.0, and SSP5-RCP8.5) and combined each with a range of disturbance regimes. Equally, we combined all disturbance scenarios with a counterfactual control climate simulation to account for interannual and decadal variability in climate. We thus simulated 16 scenarios in total (see Table 1 and Fig. 1 for an overview). To reduce dimensionality, for the purpose of this study we describe disturbance

110 regimes based on disturbance probability while keeping intensity and size constant. We chose disturbance probabilities to span from the low end of what is historically observed (return intervals of $\sim$ 300 years, see e.g. Burrell et al. (2022) and Rogers et al. (2013) to the high end of what is historically observed and projected for the future (return intervals up to 10 years, see e.g. Buma et al. (2022); Burrell et al. (2022) or Turner et al. (2019).

We simulate all gridcells within the boreal forest (taiga) biome as defined by the WWF classification of terrestrial ecoregions

115 of the world (Olson et al. (2001)) predominantly covered by needleleaf evergreen trees after the spinup period. We considered needleleaf evergreen trees to be dominant if that PFT constituted the maximum share of above-ground carbon (AGC) or fractional plant cover (FPC) in that grid cell.
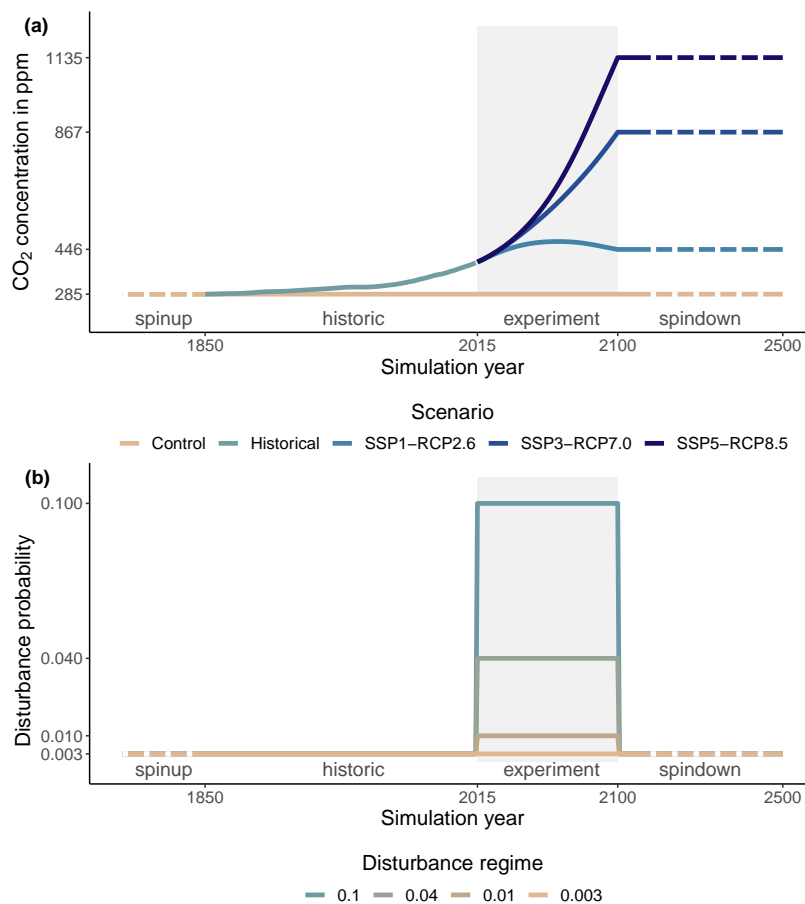
Figure 1. Overview of **(a)** simulated climate scenarios (represented by CO_2 concentration pathways) and **(b)** disturbance regimes (represented by disturbance probabilities p_D). Spinup and spindown periods (dotted lines) are not true to time scale. See also Table 1.

First, we spun the model up for 1000 years, recycling the pre-industrial climate of 1850 - 1879. During spinup, we prescribed a disturbance probability p_D of $0.00\overline{3}$ (Return interval (RI) of 300 years). We chose this low end of observed disturbance, as

120 it allows us to create a largely undisturbed but ecologically realistic setup needed to separate disturbance from climate effects during the simulation period. In the climate warming scenarios, we next simulated historical warming until the year 2015 while keeping p_D constant, after which we saved the simulation state. We then restarted the simulation from the state, running the different model configurations of climate-disturbance combinations until the year 2100. In 2100, we switched the disturbance probability back to baseline (the same as during spinup) and ran the model until 2500 to observe recovery (see Fig. 1 (b) for an

125 illustration). For this we recycled data from 2095 - 2100. In the case of the control simulations, we followed the same protocol but used counterfactual climate based on pre-industrial CO_2 concentration throughout.

Table 1. Experimental setup. In the following, we refer to different climates as *scenarios*, disturbances as *regime* or *probability*, and a climate-disturbance combination as a (model) *configuration*. See also Fig. 1.

Climate scenarios				
Scenario	Description		$\overline{\Delta T}$ in K in 2070-2100 (study region)	CO_2 in ppm in 2100
Control	Counterfactual control		0	285
SSP1-RCP2.6	Low warming, compatible with global 2° C target		3.0	446
SSP3 - RCP70	High warming		6.2	867
SSP5-RCP8.5	Very high warming		7.3	1135
Disturbance regimes				
Probability:	$0.00\overline{3}$ (*baseline*)	0.01	0.04	0.1
RI:	300	100	25	10

2.4 Data analysis

2.4.1 Vegetation composition

We analyze vegetation composition in terms of fractional plant over (FPC) and aboveground carbon (AGC). FPC describes the
130 fraction of soil covered by a specific PFT. If FPC is smaller than one, vegetation does not cover the soil completely, and the
bare soil fraction is calculated as $1 - FPC_V$. FPC can be larger than 1 in the case of dense, multi-layered vegetation. We chose
FPC as our main variable of interest as it most directly influences the later calculation of the land-surface properties albedo and
evapotranspiration. Within this study, we use the term FPC when soil fraction is included (so this can be larger than one). We
use the term 'vegetation cover' to express which percentage of vegetation FPC (excluding bare soil) consists of which PFT.

135 For clarity of analysis, we combine output for all shrub and non-woody PFTs into one vegetation type *Tundra*. Further, we
combine the PFTs BNE (*Boreal needleleaf evergreen*) and BINE (*Shade-intolerant boreal needleleaf evergreen*) to represent
all *boreal needleleaf evergreen* trees. In some instances, we additionally combine the PFTs IBS (*Shade-intolerant (pioneering)
broadleaf summergreen*) and TeBS (*Temperate broadleaf summergreen*) into one *broadleaf summergreen* category.

To account for interannual variability, the end-of-century state is represented by the mean and standard deviation over the
140 years 2085 to 2100. For all other analyses, we smooth data with a 30-year window.

We validate our simulated historical aboveground carbon against aboveground biomass from NASA's ABoVE dataset (Neigh
et al. (2013, 2015)) as carbon cycle indicators are the best-suited diagnostic variables to assess the model performance of LPJ-
GUESS.

Table 2. Characteristic albedo values Λ_i for different land cover types adapted from Boisier et al. (2013).

Land cover	Summer (Mar. - Sep.)		Winter (Oct. - Feb.)	
	snow-covered	snow-free	snow-covered	snow-free
Evergreen forest	0.205	0.104	0.205	0.094
Summergreen forest	0.244	0.117	0.244	0.153
Tundra	0.568	0.161	0.568	0.176
Soil	0.535	0.246	0.535	0.205

2.4.2 Albedo

145   We calculate monthly albedo Λ of a grid cell as the sum of the characteristic seasonal albedo values of different vegetation types Λ_i, multiplied by their respective FPC χ_i (adapted from Gregor et al. (2022) and Miller and Smith (2012)):

$$\Lambda = \sum_i^I (\chi_S \Lambda_{i,S} + \chi_0 \Lambda_{i,0}) \chi_i + (\chi_S \Lambda_{Soil,S} + \chi_0 \Lambda_{Soil,0}) \chi_{Soil} \tag{1}$$

where χ_S indicates snow-covered fraction and χ_0 snow-free fraction and

$$\chi_{Soil} = \max(0, 1 - \sum_i^I \chi_i) \tag{2}$$

150   where I is the number of PFTs.

Characteristic albedo values are taken from Boisier et al. (2013) (see also Table 2). We classify BNS trees as broadleaf summergreen as previous studies show that they are closest in specific albedo (e.g. Hollinger et al. (2010)).

LPJ-GUESS outputs the average snow depth h_S in cm. We calculate the snow cover fraction χ_S from this as

$$\chi_S = \frac{h_S}{0.1 + h_S} \tag{3}$$

155   following Wang and Zeng (2010).

2.4.3 Evapotranspiration

The model outputs monthly transpiration, soil evaporation, and leaf interception. Total evapotranspiration is calculated as the sum of the three.

2.4.4 Attribution of drivers

160 To attribute impacts to drivers in combined climate-disturbance configurations, we assume the observed total effect Δ_{SD} to be the combination of a climate effect Δ_S, a disturbance effect Δ_D, and an effect Δ_X representing interactions and other non-linearities (following Verbruggen et al. (2024)).

$$\Delta_{SD} = \Delta_S + \Delta_D + \Delta_X \tag{4}$$

We define an effect Δ_i as

165 $$\Delta_i = x_i - x_0 \tag{5}$$

where x_0 is the control model state, and x_i is the model state of a configuration i. From our factorial experiments, we can calculate Δ_S, Δ_D, and Δ_{SD} directly and Δ_X from there as

$$\Delta_X = x_0 + x_{SD} - x_S - x_D \tag{6}$$

2.4.5 Statistical testing

170 Both albedo and evapotranspiration show high interannual variability. Therefore, we performed a two-sided Wilcoxon signed-rank test on a per-gridcell basis to asses if albedo and evapotranspiration significantly differed from the configuration Control/0.003 over the years 2070 - 2100 ($p < 0.01$).

2.4.6 Tools

LPJ-GUESS simulations were performed on the CoolMuc2 Linux Cluster of the Leibniz Supercomputing Center, Munich.
175 All data analyses are executed in the `R` programming language (R Core Team (2022)) in RStudio Version 2022.12.0 using the packages `tidyverse` 1.3.2. (Wickham et al. (2019)), `furrr` 0.3.1 (Vaughan and Dancho (2022)), `sf` 1.0.9 (Pebesma and Bivand (2023); Pebesma (2018)), `terra` 1.7.3 (Hijmans (2023)), and `rnaturalearth` 0.3.2. (Massicotte and South (2023)). Plots are created with `ggplot2` (Wickham (2016)) and `cowplot` 1.1.1 (Wilke (2020)) using the Crameri color scales (Crameri et al. (2020)) as implemented by Pedersen and Crameri (2022).

3 Results

180

3.1 Vegetation composition

Following the spin-up phase, the study region's vegetation is predominantly comprised of needleleaf evergreen trees, accounting for 80 % of the AGC and 59 % of vegetation cover (here excluding bare soil fraction, see also Table B1). Broadleaf

summergreen trees (10 % of AGC and 5 % of vegetation cover) and Tundra (6 % of AGC and 34 % of vegetation cover) are
185 relevant subdominant populations in our simulations. The range of total AGC compares well to satellite-derived data (Fig. B2),
however, observed values are slightly lower and feature a pronounced peak around 3 kg/m^2 not present in the modeled data.

Keeping the disturbances constant at baseline, warming reduces the bare soil fraction from 42 % in the control scenario to
27 % in the highest warming scenario SSP5-RCP8.5 by 2100 (first bar of each block in Fig. 2A). Consequently, the fraction
of vegetation cover increases. Vegetation composition changes moderately across climate scenarios The relative contribution
190 of Tundra to vegetation cover decreases, while that of both needleleaved and broadleaf summergreen trees increases. In the
strongest warming scenario SSP5-RCP8.5, vegetation by the end of the century is composed of 69 % needleleaved trees, 21 %
broadleaved trees, and 9 % Tundra (compared to 57 %, 8 % and 34 % in control simulations). However, in terms of dominant
vegetation cover, we see little change across climate scenarios. The majority of grid cells remains dominated by needleleaf
evergreen trees, while small areas of the Southern ecotone transition to dominance of either pioneering or temperate broadleaf
195 summergreen species (first panel Fig. 2c and first column of Fig. B3).

Overall AGC increases with warming from 3.6 kgm^{-2} to 7.5 kgm^{-2} (first bar of each block in Fig. 2b). Broadleaf summer-
green trees gain above average (from 19 % to 32 % in the highest warming scenario SSP5-RCP8.5) on the expense of Tundra
and needleleaf evergreen who decrease their AGC shares from 4 % to 1 % and 75 % to 67% respectively.

In contrast, keeping climate constant but increasing disturbance probability barely affects the bare soil fraction but strongly
200 impacts vegetation composition (first block of Fig. 2a). Disturbances strongly reduce the share of needleleaf evergreen trees
until they arrive at 5 % of vegetation cover (and 3 % of total FPC when including soil) for the highest-intensity disturbance
regime of $p_D = 0.1$ in the year 2100. Tundra PFTs make up 91 % of all vegetation cover by the end of the century in this
configuration, and broadleaf summergreen trees 4 %. Consequently, the vast majority of grid cells are dominated by Tundra by
the end of the century in this disturbance regime for all climate scenarios (center panel of Fig. 2c, and right column in Fig. B3).
205 AGC is strongly reduced by disturbances from 3.6 kgm^{-2} to 0.5 kgm^{-2} for the highest disturbance intensity (first block of
Fig. 2b). This happens mainly at the expense of trees, while Tundra PFTs gain carbon in both relative and absolute terms.

We see different dynamics in the case of the combined climate-disturbance configurations. In a warmer climate, an increase
in disturbance leads to a further reduction of bare soil, for example, reaching 24 % in the high-warming/high-disturbance
configuration SSP5-RCP8.4/0.04, compared to 27 % through high warming alone (Fig. 2a). For the highest disturbance proba-
210 bility of 0.1, soil fraction increases again to 30 %. In terms of vegetation composition, the disturbance-induced replacement of
needleleaf evergreen trees with Tundra remains the dominant pattern. However, we see the opposing warming-induced increase
of broadleaf summergreen trees, which is further exacerbated by disturbance. This increase is non-linear, reaching its peak for
the second-highest disturbance regime $p_D = 0.04$, where broadleaf summergreen trees make up 32% of vegetation cover and
24 % of total FPC (compared to 21 % and 15 % respectively through warming alone). For the highest disturbance scenario
215 of 0.1, the share of broadleaf summergreen trees is again comparable to the baseline disturbance. We see a similar effect in
terms of AGC, where broadleaf summergreen species, for example, make up 54 % of AGC in the combined SSP5-RCP8.5/0.04
configuration by 2100, compared to 32 % through warming alone.
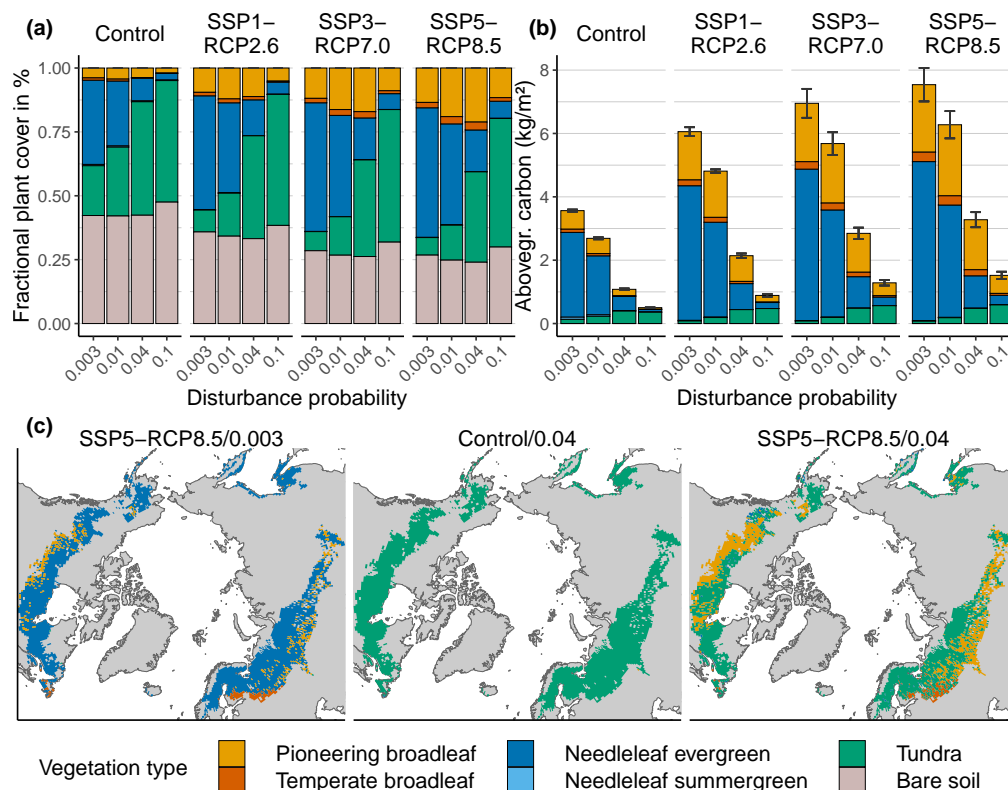
Figure 2. End-of-century vegetation composition across the study domain. **(a)**: Mean FPC by PFTs for all scenarios across the study domain. Mean vegetation FPC is always smaller than 1, and bare soil fraction is calculated as $1 - FPC_V$. Therefore, absolute FPC equals relative FPC **(b)**: Above ground carbon (AGC) per PFT and model configuration. Bars indicate mean over years 2700 - 2100; error bars standard deviation. **(c)**: Spatial patterns of end-of-century dominant vegetation (defined as the largest share of FPC per grid cell) exemplary for a high-warming/control-disturbance (left), control-climate/high-disturbance (middle) and high-warming/high-disturbance configuration (right).

The higher absolute and relative share of pioneering broadleaves translates to a shift towards broadleaf summergreen dominance in distinct, mostly southern regions of the study domain (right panel in Fig. 2c). The number of such shifts increases

220 with disturbance and climate (Fig. B3). The majority of remaining grid cells remain at needleleaf evergreen dominance for a p_D of 0.01 and transition to Tundra dominance for a p_D of 0.04.

To further disentangle the role of the different drivers in the combined configuration, we next perform the factorial attribution and investigate the relative contribution of drivers over time 3. We here focus on the configuration SSP5-RCP8.5/0.04 that showed the strongest interaction effect between climate and disturbance.

225 The combined effect of climate and disturbance on vegetation plant cover (total effect Δ_{SD}) in this configuration steadily increases over the scenario period (years 2015 - 2100), reaching its maximum of 0.2 (read: an additional share of total FPC of 20 %) at the end of the scenario period (black line in the first panel of Fig. 3). This is larger than the pure climate effect Δ_S reaching peak levels of 0.17 (blue line in Fig. 3a), despite disturbances alone not affecting vegetation cover (green line

Table 3. Comparison of simulated monthly values for albedo and evapotranspiration under control/ historical climate to observed values.

Albedo	DJF	JJA	
Own simulations	**0.33**	**0.18**	
Kim et al. (2024)	-	0.21	*North America, ABoVE domain, pre-fire*
Potter et al. (2020)	0.31	0.11	*North America, 60 years after disturbance*
Rogers et al. (2013)	0.33	0.08	*North America, mature forest stands*
Kiljunen (2006)	0.35	0.12	*Finnland, needleaf evergreen stands*
ET in mmmonth^{-1}	DJF	JJA	
Own simulations	**0.3**	**69.0**	
Wang et al. (2021)	3.7	83.4	*circumboreal, 1982–2015 mean, modelled*
Ju et al. (2010)	6.8	73.9	*Canada, various sites, Eddy covariance*

in Fig. 3a). Consequently, there exists an interaction effect Δ_X between climate and disturbance (pink line in Fig. 3a) that

230 increases steadily over the scenario and reaches peak levels of 0.1.

The dynamics of different vegetation types vary quite strongly. At the end of the simulation period, the total effect on needleaf evergreen fraction is a decrease of -0.19. This is the net of a disturbance-induced decrease of -0.25, a climate-induced increase of 0.16, and an interaction effect of -0.1. In contrast, the total increase in Tundra fraction of 0.15 at the end of the simulation period consists of a disturbance-induced increase of 0.26, a climate-induced decrease of -0.12, and an interaction

235 effect of 0.01 (but note that interactions are larger during and after the simulation period.

The picture is different for broadleaf summergreen trees. Here, the total effect Δ_{SD} of an additional 0.24 in fractional cover is larger than the climate-induced increase of 0.13 while the pure disturbance effect is 0. For broadleaf trees, we consequently see the strongest interaction effect of 0.11 by 2100 and a maximum effect of 0.46 in the year 2141 (read: an additional increase of 0.46 in broadleaf FPC due to interactions between disturbances and climate).

240 The increase in total vegetation FPC reverses slightly after disturbances are set back to baseline in 2100 and reaches stable values of 0.1 after 200 years. Tree FPC stabilizes around the same time, with needleaf evergreen trees reaching a final Δ_{SD} of -0.17 and broadleaf summergreen trees of 0.28. At this point, disturbance-induced effects become marginal, by the end of the simulations, they have disappeared completely, and the total effect converges again with the pure climate effect Δ_S.

Tundra FPC follows a different dynamic during the spindown phase. Once disturbances are set back to baseline in 2100,

245 FPC sharply decreases, and the total effect Δ_{SD} becomes negative a few years into the spindown period. By the end of the simulation, it has stabilized at -0.15. Interestingly, the interaction effect Δ_X follows a similar pattern: positive during the scenario period but negative during early spindown and disappearing around the simulation year 2300.

By the end of the simulation (year 2500), all disturbance-related effects have disappeared ($\Delta_{SD} = \Delta_S, \Delta_D = 0, \Delta_X = 0$), and vegetation is in equilibrium again ($\Delta_{SD} = const$).
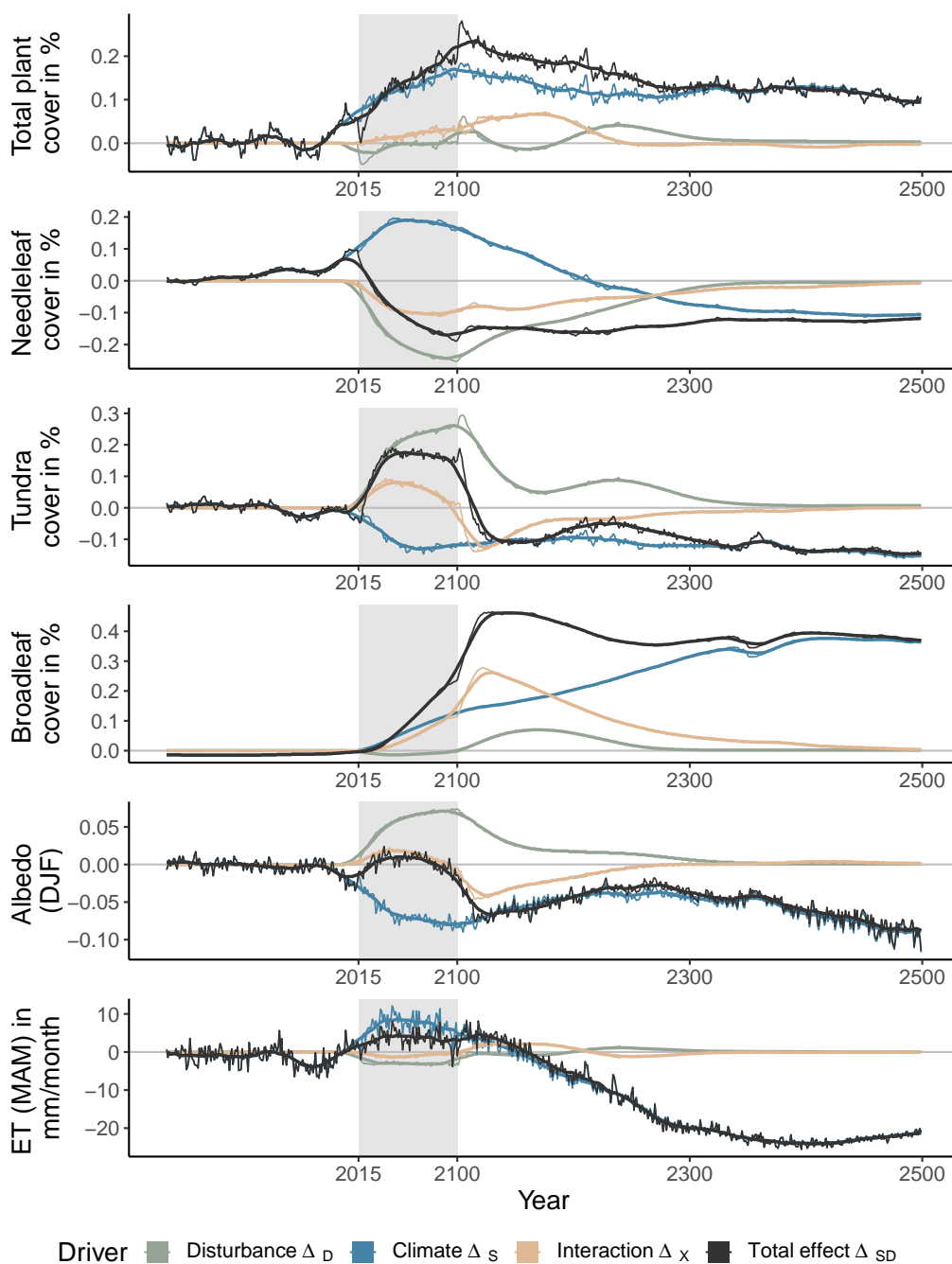
Figure 3. Total effects relative to control conditions and their attribution to different factors for vegetation composition, albedo, and evapotranspiration for the model configuration SSP5-RCP8.5/0.04. Grey boxes indicate the scenario period during which the disturbance regime is changed.

3.2 Surface properties

3.2.1 Albedo

Albedo exhibits pronounced seasonality. Under control conditions, it reaches peak values of 0.36 ± 0.005 in March and minimum values of 0.18 ± 0.01 in October(Fig. 4a). Simulated winter albedo agrees well with recent observations, while summer albedo in our study is on the high end of observations (see Table 3). Warming alone decreases albedo, especially in winter, where maximum values at the end of the century are reduced to 0.33 ± 0.003 in the low warming scenario SSP1-RCP2.6 and by 0.25 ± 0.005 in the highest warming scenarios SSP5-RCP8.5 (solid light and dark blue in Fig. 4a). The seasonal amplitude in albedo decreases with warming, from 0.18 ± 0.006 in the control climate to 0.16 ± 0.002 in a low-end warming scenario (SSP1-RCP2.6) and 0.14 ± 0.001 in a high-end warming scenario (SSP5-RCP8.5). Albedo reductions are visible throughout the study region. There are, however, spatial variations in magnitude, with distinct patches of strong anomalies in Eastern Canada and Eurasia, while other areas, especially in Western Canada, Alaska, and Southern Russia, show very little change (left panel in Fig. 4c).

An increase in disturbance intensity alone has the opposite effect. Increasing p_D from 0.003 to 0.04 while keeping climate constant increases winter albedo to 0.40 ± 0.005 in winter and to 0.21 in summer (dashed pink line in Fig. 4a and pink bars in Fig. 4b). The seasonal amplitude increases to 0.23. The magnitude of change is more uniform throughout the study region (center panel in Fig. 4c).

In the combined scenarios, the pattern of increasing albedo with disturbance intensity and decreasing albedo with warming is preserved. However, the net effect differs between scenarios. For the moderate increase in disturbance intensity $p_D = 0.01$, the climate effect prevails, resulting in a net decrease in albedo (second group in Fig. 4b). For the highest-intensity disturbance regime $p_D = 0.1$, the disturbance effect is stronger, leading to a net increase in albedo compared to baseline disturbance (right group in Fig. 4b). In the middle case of $p_D = 0.04$, we observe a net increase for the SSP1-RCP2.6 scenario and a slight net decrease for the SSP5-RCP8.5 scenario. In the winter months SSP5-RCP8.5/0.04 is almost at par with the control/baseline configuration (dashed dark blue line in Fig. 4a). This change is not uniform across the domain (right panel in Fig. 4c). The climate-disturbance configuration SSP5-RCP8.5/0.04, for example, shows an albedo increase in distinct regions and decreases in others, resulting in the small net change visible in Fig. 4a and B. While the pure climate- and disturbance effect results in significant changes in the majority of the study region, the combined effect can not be separated from interannual variability in this particular configuration.

When investigating the different albedo drivers over time, again for the example configuration SSP5-RCP8.4/0.04, shows that the climate and disturbance effects constantly increase over the scenario and maintain comparable orders of magnitude but in different directions. At the end of the scenario period, the climate effect is -0.079, and the disturbance effect is 0.068. The interaction effect is small at this point (-0.01). The total albedo effect is, therefore, negligible for most of the scenario ($<$ 0.01), only declining in the last decade of the scenario period to reach -0.023 in 2100. These trends are reversed after the end of the scenario. Δ_{SD} converges with Δ_S while Δ_D declines but only approaches 0 after the year 2300. Consequently, we see a counteracting interaction effect until this point as well. The final net albedo effect in simulation year 2500 is -0.088.

3.2.2 Evapotranspiration

285 Like albedo, evapotranspiration shows high seasonality (Fig. 5a). For all configurations, evapotranspiration is low (< 1 mm/-month) in winter (DJF) and reaches highest levels in July. Peak evapotranspiration reaches 69 ± 2 mm/month in the control/baseline scenario. Additionally, evapotranspiration shows the strongest interannual variation. Our simulated values are slightly lower than observations but capture the seasonal amplitude well (see Table 3).

Warming alone increases evapotranspiration. The strongest effect is seen in spring, where ET increases by about $4.9 \pm$ 290 2.3 mm/month for the low-end warming scenario SSP1-RCP2.6 and 10.2 ± 3 mm/month in the highest warming scenarios SSP5-RCP8.5 (solid light and dark blue in Fig. 5a and left group in Fig. 5). Notably, maximum evapotranspiration does not differ between the low-end and the high-end warming scenario (76.4 ± 2 mm/month and 76.5 ± 3 mm/month respectively). Climate-induced change in evapotranspiration is seen across the study domain, but the magnitude varies (first panel of Fig. 5c). The strongest decrease is seen in Eastern Canada and South-Eastern Russia.

295 Disturbance alone decreases evapotranspiration (dashed pink line in Fig. 5a and pink bars in Fig. 5), for the most intense disturbance regime by -3.47 ± 0.25 mm/month. This decrease is concentrated in distinct areas, while most of the study regions shows no significant change (middle panel of Fig. 5c).

For the majority of combined climate-disturbance configurations, the net effect is an increase in evapotranspiration (Fig. 5b). The exception is SSP1-RCP2.6/0.1 (low-end warming scenario), where evapotranspiration remains unchanged from baseline, 300 as the climate and disturbance effects offset each other. The spatial analysis shows that, again, evapotranspiration increases in most areas (right panel of Fig. 5 for SSP5-RCP8.5/0.04). However, there are distinct areas that show no significant change. Maximum evapotranspiration is 72.3 ± 2.8 mm/month and 72.7 ± 2.6 mm/month for the SSP1-RCP2.6 and SSP5-RCP8.5 scenarios respectively and for a p_D of 0.04 (dashed blue lines in Fig. 5a).

Drivers of evapotranspiration effects over time show similar patterns to albedo but in reversed directions. Again, for the 305 example configuration SSP5-RCP8.5/0.04, climate increases evapotranspiration with peak levels of $+8.5$ mm/month around the year 2050, while disturbances reduce evapotranspiration. Contrary to albedo, Δ_D is smaller in magnitude than Δ_S, and the net effect over the scenario period is therefore positive, reaching 3.1 mm/month at the end of the scenario. There is no interaction effect. The disturbance effect declines immediately after the end of the scenario. Δ_S and Δ_{SD} reverse and become negative around 50 years after the scenario period. The final effect at the end of the simulation period is -24 mm/month.

310 ## 4 Discussion

4.1 Vegetation composition

Historical species distributions produced by our model are in line with observational data and previous modeling studies performed with LPJ-GUESS (see e.g., discussion of Zhang et al. (2013) or Wolf et al. (2008)), and the range of total AGC corresponds to observations (Fig. B2). The slightly higher total AGC in our simulations is due to the fact that we simulate potential 315 natural vegetation and do not consider impacts of land use change or harvest, which is especially important in Scandinvia and
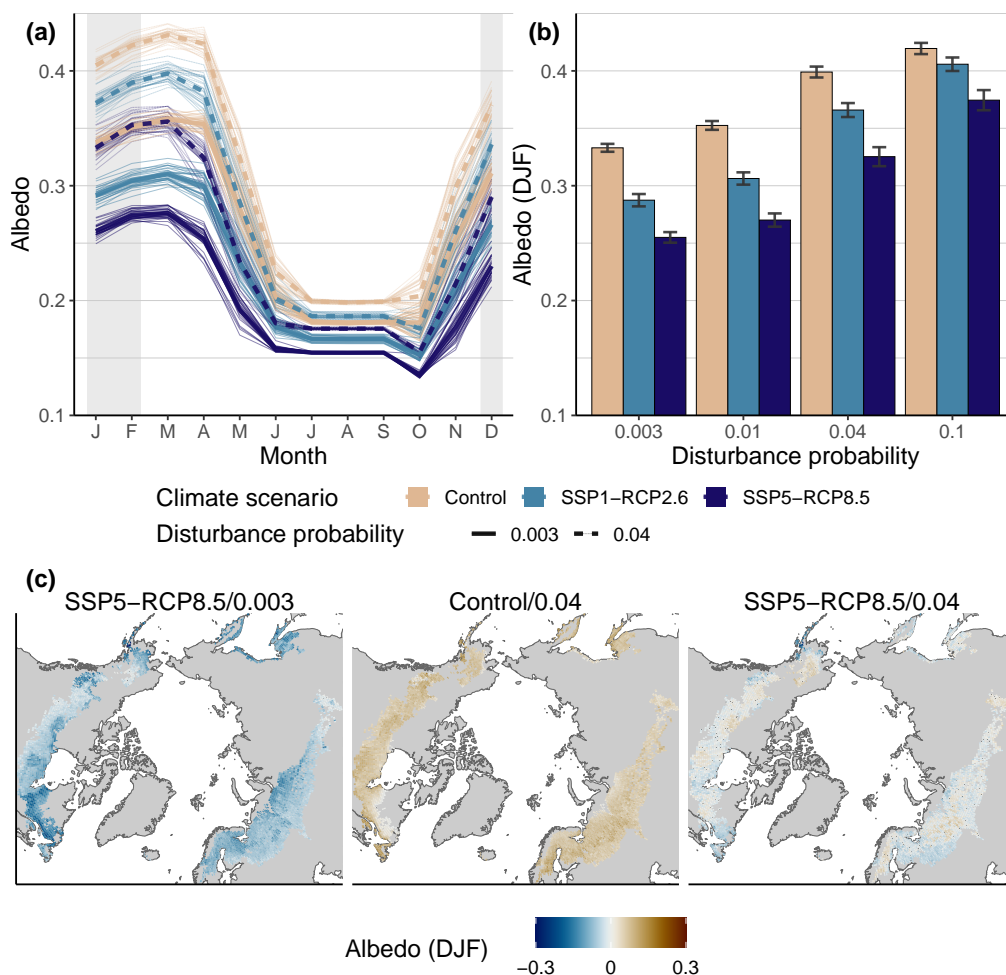
Figure 4. End of century albedo across the study domain. **(a)**: Seasonal albedo for selected configurations. Pink lines indicate control climate and blue lines show low-end (light blue) and high-end (dark blue) warming. Solid lines indicate baseline disturbance regimes, dashed lines a p_D of 0.04. Thick lines show mean over 2070 - 2100, thin lines individual years. **(b)**: Winter (DJF) albedo for a range of configurations. Bars indicate mean over the years 2070 - 2100, error bars ± one standard deviation. **(c)**: Spatial patterns of albedo anomaly (relative to control/baseline) for a high-warming/control-disturbance (left), control-climate/high-disturbance (middle) and high-warming/high-disturbance configuration (right). Stiples indicate areas where albedo does not significantly differ from configuration Control/0.003 ($p < 0.01$).
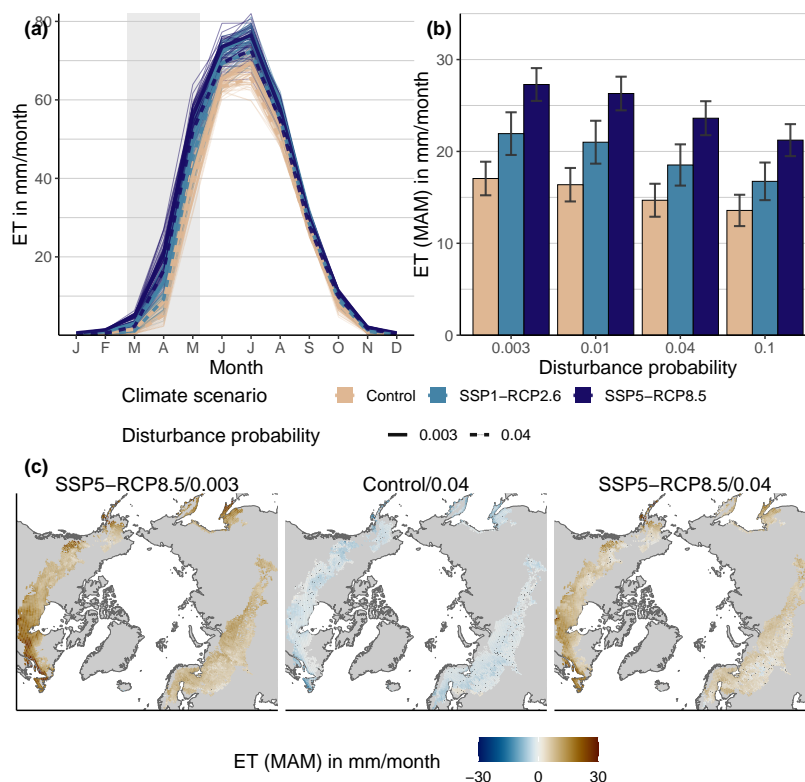
Figure 5. End of century evapotranspiration (ET) across the study domain. **(a)**: Seasonal ET for selected configurations. Pink lines indicate control climate, blue lines show low-end (light blue) and high-end (dark blue) warming. Solid lines indicate baseline disturbance regimes, dashed lines a p_D of 0.04. Thick lines show mean over 2070 - 2100, thin lines individual years. **(b)**: Spring (MAM) ET for a range of configurations. Bars indicate mean over the years 2070 - 2100, error bars ± one standard deviation. **(c)**: Spatial patterns of ET anomaly (relative to control/baseline) for a high-warming/control-disturbance (left), control-climate/high-disturbance (middle) and high-warming/high-disturbance configuration (right). Stipples indicate areas where evapotranspiration does not significantly differ from configuration Control/0.003 ($p < 0.01$).

Canada (Pugh et al. (2019b); Potapov et al. (2017); Curtis et al. (2018)). Additionally, disturbance frequency during spinup is lower than what is observed in some areas since we aim for largely undisturbed vegetation at the start of the scenario to be able to separate disturbance from climate effects during the scenario period. However, vegetation under historical climate is robust in our model against a change in disturbance probability within historical return intervals that rarely exceed the 100 - 50 year

320 range (Fig. 2, Burrell et al. (2022); Rogers et al. (2013)). Therefore, it is reasonable to assume that our simulations represent a realistic ecological state.

In general we find that climate is the dominant driver of the increase in total vegetation cover and carbon, while a complex interplay between climate, disturbance and their interactions mediates changes on the PFT level and thus vegetation composition. Climate change induces an increase in needleleaf evergreen tree cover at the expense of Tundra, as warming favours

325 the expansion and northward migration of trees (Boulanger and Pascual Puigdevall (2021); Gustafson et al. (2021); Rees et al. (2020); Zhang et al. (2013)) while disturbances have the opposite effect, decreasing needleaf evergreen tree cover and increasing that of Tundra in our simulations. Depending on the combination of climate and disturbance regime employed, we thus can find a net replacement of Tundra with needleleaved trees, the opposite or diverging trends in different regions. In the case of broadleaved trees, climate change favours their expansion, while disturbance does not affect their FPC share. In the absence of

330 interaction effects, disturbance thus does not affect total vegetation cover, since the replacement of needleleaf evergreen trees with Tundra results in zero net change. Climate in turn has a net positive effect, as the expansion of both needleleaf evergreen and broadleaf summergreen trees exceeds what is being replaced in Tundra.

The interaction between climate and disturbance leads to a combined response that for needleleaf evergreen trees and Tundra is closer to the sole disturbance effect as would be expected. However, for Tundra this is reversed after the scenario end and

335 disturbance effects quickly disappear. Both can be explained by the strong expansion of broadleaf summergreen trees in the combined scenarios. Broadleaf trees substitute both needleleaf evergreen tree and Tundra after disturbance, preventing their respective climate- and disturbance-driven expansion. Given the assumption that future disturbance rates will significantly surpass historical levels, a decline in needleleaf evergreen tree cover is likely. This is also in line with trends observed over the last decades, e.g. by Wang et al. (2020), who observed a decrease in needleleaf evergreen tree cover and an increase in

340 broadleaf summergreen trees and Tundra over the years 1984–2014.

Spatial patterns of broadleaf summergreen tree dominance in our simulations correspond to observations from recent field surveys in North America that report such vegetation shifts predominantly in Alaska and Western Canada, while the Eastern Canadian Shield and Plains show higher rates of recovery and shifts between different needleleaved species (Baltzer et al. (2021)). Our model additionally projected state shifts in Southern Russia in our simulations, from where comparable field

345 surveys are still lacking. Pioneering broadleaves, such as Aspen or Birch species, are an integral part of succession cycles in many ecosystems of the boreal region (Pfadenhauer and Klötzli (2020)). Thus, one might anticipate there expansion at elevated elevated disturbance levels solely based on a higher proportion of vegetation in an early-successional state in the model. However, when the disturbance rate was increased under a controlled climate, it had minimal impact on these species' absolute or relative abundance. Consequently, their rise cannot be solely attributed to this. Instead, a shift in climatic conditions

350 is additionally needed to render broadleaved species more competitive in post-disturbance recovery (Baltzer et al. (2021); Mekonnen et al. (2019); Warlind et al. (2014)).

An effect that might not be expected at first glance is the resilience of total vegetation FPC to disturbance, as reduction of vegetation density due to high disturbance is likely. We explain this finding in our simulations through the replacement of tree cover with Tundra. Therefore, while aboveground biomass rapidly decreases, FPC increases due to the higher relative leaf area

355 of Tundra PFTs. This also explains the increase of vegetation cover and reduction of bare soil with increasing disturbance rate. Undisturbed vegetation composition in our simulations is remarkably resilient against climate change, which also corresponds to recent observations (Kim et al. (2024); Sulla-Menashe et al. (2018)). The same is not true of AGC, which is strongly diminished by disturbances. Again, this affects mainly needleleaf evergreen trees, while broadleaf summergreen trees and Tundra PFTs are resilient to disturbance and increase their AGC share, also in line with recent field observations (Baltzer

360 et al. (2021); Mack et al. (2021)). As our analysis focuses on above-ground processes, it does not allow for further conclusion regarding the impact on the boreal carbon balance, where belowground processes play an important role.

Overall, our results suggest that modeling results of future vegetation distributions are highly sensitive to the choice of disturbance regime. Therefore, without an accurate representation of disturbance regimes, there is the danger of overestimating the stability of future vegetation. Due to the interaction effects between climate and disturbances, this sensitivity becomes

365 increasingly important with warming, while historical simulations are more robust.

4.2 Land surface properties and potential climate feedbacks

Our simulated historical albedo is high compared to observations in summer, while winter albedo, the main focus of our analysis, shows high agreement. Our results indicate that disturbance and climate have significant but opposing effects on albedo. Therefore, depending on the climate-disturbance configuration, we may see a net increase, decrease, or little net change.

370 Previous modeling studies such as Krause et al. (2019), Zhang et al. (2018) or Zhang et al. (2013) predominantly found albedo decreases of up to -0.25, depending on the climate scenario employed and specific region. This corresponds to our finding for a moderate disturbance scenario (Fig. 4b, second group). These studies did not explicitly consider the effects of disturbance, and the assumed disturbance rates are not always reported. However, it is likely that their results predominantly capture climate effects. Our results indicate that albedo decreases may be reduced or even reversed in a high-disturbance world.

375 Vegetation shifts are the main driver of albedo change, most importantly the relative shifts between Tundra and needleleaf evergreen tree cover. Contrary to what previous studies have postulated (Baltzer et al. (2021); Wang and Friedl (2019); Rogers et al. (2013)), the strong increase in broadleaf summergreen tree cover, which we found in our simulations especially between the years 2100 and 2200, does not translate to an albedo increase. This can by explained by the fact the broadleaf summergreen tree expansion occurs also at the expense of Tundra and bare soil, which have higher specific albedo. It should be noted that

380 the calculated albedo values are highly dependent on the specific albedo values used (Table 2). The values we used were not derived specifically for the boreal forest, and it is possible that they underestimated the difference in albedo between vegetation types. Indeed, some studies report albedos of 0.6 - 0.8 in early-successional and/ or broadleaf summergreen forest stands (Kim et al. (2024); Zhang et al. (2018); Rogers et al. (2013)). Such values would be unattainable with our approach. In other studies,

however, albedo values are in line with our findings, e.g. mean albedo values after disturbance not exceeding 0.5 in Potter et al.
385 (2020). All these studies report albedo values at site level, representing a mixture of different vegetation types and soil that are not directly translatable to specific albedo values. If specific albedos for the boreal forest were available, they would greatly improve the accuracy of albedo calculations in the future.

Snow cover dynamics drive the season albedo amplitude but play a minor role for albedo changes in the climate scenarios. This might seem surprising at first since one might intuitively expect reduced snow cover due to warming. In LPJ-GUESS,
390 warming results in earlier snowmelt and later onset of the snow season over the study area, while snow cover during winter was barely affected by warming (Fig. B4a). This is expected from the climate forcing data used (Fig. B1) and in line with 21st-century projections from CMIP5 and CMIP6 as well as previous results from dynamic vegetation models (McCrystall et al. (2021); Krause et al. (2019); Krasting et al. (2013)). Uncertainties regarding future snow cover in the climate data used will, of course, in turn, influence our albedo calculations. We here also want to note that Potter et al. (2020) found snow
395 cover an important predictor of post-fire albedo changes when combining statistical analysis of recent fire events with climate projections.

Evapotranspiration shows opposite patterns from albedo, as here climate leads to an increase, while disturbance leads to a decrease. Additionally, in contrast to albedo, the magnitude of change is larger for climate-induced increases. Therefore - within the realistic parameter space assessed in this study - there is no configuration that would achieve a net decrease in
400 evapotranspiration. However, the net effect can be significantly reduced compared to the pure climate effect.

The impact of disturbances on evapotranspiration is less well-studied than that of albedo. Previous modeling studies found overall increases in evapotranspiration throughout our study domain (Krause et al. (2019); Zhang et al. (2013)), even though Krause et al. (2019) found diverging signals when comparing several DVMs. Again, from our results, we can expect those changes to be reduced when accounting for a high-disturbance future.

405 Climate-driven evapotranspiration change can occur due to both direct climate effects such as temperature or precipitation increase, CO_2-mediated changes in water use efficiency, and climate-modulated vegetation change, which is challenging to untangle. As temperature and precipitation both increase over the course of the scenario, it is likely that climate-induced changes are at least partly driven by direct climate effects. However, as climate is held constant after 2100 we can assume any changes taking place after that to be modulated by vegetation.

410 We expected an increase in evapotranspiration after disturbance due to a higher share of broadleaf summergreen trees and, in turn, higher Leaf Area Index (LAI), something we cannot confirm from our results. From the individual components making up evapotranspiration, it appears to us that the reduction of needleleaf evergreen tree cover reduces interception and increases runoff, especially in spring, and thus leads to less water being available for evapotranspiration (Fig. B5). Other studies investigating evapotranspiration after fire disturbance equally found reductions both in the field (Liu et al. (2018)) and in modeling
415 results (Bond-Lamberty et al. (2009)). It should be noted that ecophysiological control on ET is relatively weak in the current version of LPJ-GUESS. Current and future model development that takes into account different hydraulic strategies of PFTs is likely to change results in this regard (Papastefanou et al. (2020, 2022); Meyer et al. (2024)).

An increase in both albedo and evapotranspiration would result in a cooling of the land surface, while a decrease would have a reversed effect. As LPJ-GUESS was not coupled to an atmospheric model, we cannot determine the actual net effect,

420 especially as other processes, such as cloud formation or surface roughness, can additionally play a role (Gregor et al. (2022); Swann et al. (2010)). Previous coupled studies with LPJ-GUESS report a net warming effect due to vegetation dynamics with a high degree of intra-annual and spatial variations (Zhang et al. (2018)). Our results indicate that accounting for an increase in disturbances and resulting vegetation changes are lightly to weaken that effect.

4.3 Legacy effects and resilience

425 We find that disturbance-induced effects on vegetation are long-lasting (∼ several 100 of years) but ultimately transient and reversible on the centennial time scale if disturbance pressure is lifted again. Tree cover fraction takes the longest to recover, where the total effect converges again with the undisturbed trajectory after up to 400 years.

Of course, our stylized scenarios are not a likely long-term scenario as return to baseline disturbance regimes after 2100 is very unlikely. The change would most likely be sustained with a sustained level of disturbance frequency. The question of

430 reversibility is nevertheless relevant in the context of forest management and climate mitigation. Our results also confirm that the end-of-century vegetation state does not represent an equilibrium, as already shown by e.g. Pugh et al. (2018).

However, recovery patterns need to be interpreted cautiously, as there are a number of limitations in the implementation of establishment and disturbance in the model: In LPJ-GUESS there is no interaction between gridcells for reasons of computational efficiency and thus there is no lateral exchange of seeds, that would control spatial migration. Rather, migration is

435 emulated through a background establishment rate, a small rate of establishment that will always occur as soon as PFTs are within their bioclimatic limits. This may lead to a faster northward expansion of trees than if migration would be limited by seed dispersal (Zani et al. (2023)). Additionally, the production of offspring and thus establishment can occur once a plant is productive, there is no maturation period. This means that regeneration failure - eroding of seed banks through too frequent disturbances (Turner et al. (2019); Hansen et al. (2018)) - cannot occur by model design. Here, different reproductive strategies,

440 e.g. serotony or resprouting, would also be important to consider (Baltzer et al. (2021); Hansen et al. (2021)).

In this context, disturbance type is also important. We here employed a standardized disturbance event to reduce dimensionality in our simulations and ensure controlled experiments. However, it is important to keep in mind that specific disturbances can have additional effects we are not considering here. For example, wildfire affects soil conditions, e.g. through the burning of the peat layer and changes in nutrient cycling (Mack et al. (2021); Mekonnen et al. (2019)). Further, our disturbance dynamics

445 are neither linked to climate nor to vegetation type, as, for example, a detailed fire disturbance module would be. In that case, we would especially expect disturbance frequency and impact to differ with vegetation type. Broadleaf summergreen trees are less susceptible to fire, and literature suggests that broadleaf summergreen tree dominance could maintain itself through fire suppression (Hansen et al. (2021); Mekonnen et al. (2019); Johnstone et al. (2016, 2010)). Wind damage and pathogen attacks are equally linked to climate conditions and species compositions (Mitchell (2013); Seidl et al. (2017)). Taken together, all

450 these limitations suggest a potential overestimation of the recovery ability of vegetation in the model.

Disturbance-induced changes in land-surface properties are mainly driven by changes in Tundra cover, less subject to legacy effects and internal dynamics than tree cover and more directly controlled by climate. Therefore, both albedo and evapotranspiration recover quickly once disturbance pressure is lifted again, and legacy effects disappear after approximately 25 years. We stress that our results inform on the potential ability to recover rather than a realistic projection of likely dynamics after the

455   21st century. With sustained disturbance regimes, the respective changes in land-surface properties would likely persist.

5   Conclusions

In this study, we investigated the relative impact of climate change, intensifying disturbance regimes, and their interaction on boreal vegetation and land surface properties. We found that in general climate drives shifts towards denser and more forested vegetation, while disturbances reduce the prevalence of trees in favor of shrubs and grasses. The interaction between climate

460   and disturbances increases broadleaf summergreen tree cover, causing shifts from needleleaf evergreen and Tundra to broadleaf summergreen dominance. The shifts we observe are not driven by prescribed bioclimatic limits but are an emergent feature of the model, arising from a shift in competitive balance. This highlights the ability of LPJ-GUESS to realistically capture the influence of climate change on succession and thus post-disturbance recovery dynamics.

In our simulations, disturbances affect albedo and evapotranspiration. In both cases, the disturbance effect opposed the

465   pure climate effect, while interactions between the two factors played a minor role. ET is more closely coupled to direct climate effects, with vegetation changes playing a subordinate role. In contrast, vegetation shifts (due to both disturbances and warming) are the main driver of observed albedo changes. Here, disturbance-induced effects have the potential to weaken or even reverse climate-induced changes.

Disturbances caused long-lasting legacies in vegetation composition, which only regenerated on the centennial time scale.

470   On the opposite, albedo and evapotranspiration recovered on a decadal timescale. Therefore, while our results show the ability for disturbances to severely disrupt land surface-atmosphere interactions, they also highlight the potential for regeneration.

We find simulated future vegetation distributions highly sensitive to the choice of disturbance regime. Due to the interaction effects between warming and disturbances, this sensitivity becomes increasingly important when moving into a high-warming future, while historical simulations are more robust against the choice of disturbance regime. Without an accurate representation

475   of disturbance, there is a risk of misjudging future vegetation composition and resulting land surface properties.

Code and data availability.   LPJ-GUESS model code and raw model output are archived on Zenodo (https://doi.org/10.5281/zenodo.10619524). The code to reproduce the analyses and figures is found on Github (https://github.com/lucialayr/disturbanceBorealLPJ).

Author contributions.   LSL and AR designed the study. LSL performed the model simulated and data analyses and prepared the manuscript. KG, AK and PM contributed to model development and setup. All authors contributed to the interpretation of the results and the revision of

480   the manuscript.

Competing interests. At least one of the (co-)authors is a member of the editorial board of Biogeosciences. The authors declare no further conflict of interest.

Acknowledgements. LSL is supported by a PhD fellowship from the German Federal Ministry of Education and Research, issued via the Heinrich Boell Foundation. LSL and AK acknowledge support from the German Federal Ministry of Education and Research via the
485   STEPSEC project, grand number 01LS2102C. KG acknowledges funding from the VELUX foundation, Project No. 1897. The authors acknowledge the use of Grammarly and ChatGPT for English grammar and language support.

References

Alexander, H. D., Mack, M. C., Goetz, S., Beck, P. S. A., and Belshe, E. F.: Implications of increased deciduous cover on stand structure and aboveground carbon pools of Alaskan boreal forests, Ecosphere, 3, art45, https://doi.org/10.1890/ES11-00364.1, 2012.

490 Allen, C. D., Macalady, A. K., Chenchouni, H., Bachelet, D., McDowell, N., Vennetier, M., Kitzberger, T., Rigling, A., Breshears, D. D., Hogg, E. T., Gonzalez, P., Fensham, R., Zhang, Z., Castro, J., Demidova, N., Lim, J.-H., Allard, G., Running, S. W., Semerci, A., and Cobb, N.: A global overview of drought and heat-induced tree mortality reveals emerging climate change risks for forests, Forest Ecology and Management, 259, 660–684, https://doi.org/10.1016/j.foreco.2009.09.001, 2010.

Baltzer, J. L., Day, N. J., Walker, X. J., Greene, D., Mack, M. C., Alexander, H. D., Arseneault, D., Barnes, J., Bergeron, Y., Boucher, Y.,
495 Bourgeau-Chavez, L., Brown, C. D., Carrière, S., Howard, B. K., Gauthier, S., Parisien, M.-A., Reid, K. A., Rogers, B. M., Roland, C., Sirois, L., Stehn, S., Thompson, D. K., Turetsky, M. R., Veraverbeke, S., Whitman, E., Yang, J., and Johnstone, J. F.: Increasing fire and the decline of fire adapted black spruce in the boreal forest, Proceedings of the National Academy of Sciences, 118, e2024872118, https://doi.org/10.1073/pnas.2024872118, 2021.

Boisier, J. P., de Noblet-Ducoudré, N., and Ciais, P.: Inferring past land use-induced changes in surface albedo from satellite observations: a
500 useful tool to evaluate model simulations, Biogeosciences, 10, 1501–1516, https://doi.org/10.5194/bg-10-1501-2013, 2013.

Bonan, G. B.: Forests and Climate Change: Forcings, Feedbacks, and the Climate Benefits of Forests, Science, 320, 1444–1449, https://doi.org/10.1126/science.1155121, 2008.

Bond-Lamberty, B., Peckham, S. D., Gower, S. T., and Ewers, B. E.: Effects of fire on regional evapotranspiration in the central Canadian boreal forest, Global Change Biology, 15, 1242–1254, https://doi.org/10.1111/j.1365-2486.2008.01776.x, 2009.

505 Boulanger, Y. and Pascual Puigdevall, J.: Boreal forests will be more severely affected by projected anthropogenic climate forcing than mixedwood and northern hardwood forests in eastern Canada, Landscape Ecology, 36, 1725–1740, https://doi.org/10.1007/s10980-021-01241-7, 2021.

Brice, M., Vissault, S., Vieira, W., Gravel, D., Legendre, P., and Fortin, M.: Moderate disturbances accelerate forest transition dynamics under climate change in the temperate–boreal ecotone of eastern North America, Global Change Biology, 26, 4418–4435,
510 https://doi.org/10.1111/gcb.15143, 2020.

Buma, B., Hayes, K., Weiss, S., and Lucash, M.: Short-interval fires increasing in the Alaskan boreal forest as fire self-regulation decays across forest types, Scientific Reports, 12, 4901, https://doi.org/10.1038/s41598-022-08912-8, 2022.

Burrell, A. L., Sun, Q., Baxter, R., Kukavskaya, E. A., Zhila, S., Shestakova, T., Rogers, B. M., Kaduk, J., and Barrett, K.: Climate change, fire return intervals and the growing risk of permanent forest loss in boreal Eurasia, Science of The Total Environment, 831, 154885,
515 https://doi.org/10.1016/j.scitotenv.2022.154885, 2022.

Calvin, K., Dasgupta, D., Krinner, G., Mukherji, A., Thorne, P. W., Trisos, C., Romero, J., Aldunce, P., Barrett, K., Blanco, G., Cheung, W. W., Connors, S., Denton, F., Diongue-Niang, A., Dodman, D., Garschagen, M., Geden, O., Hayward, B., Jones, C., Jotzo, F., Krug, T., Lasco, R., Lee, Y.-Y., Masson-Delmotte, V., Meinshausen, M., Mintenbeck, K., Mokssit, A., Otto, F. E., Pathak, M., Pirani, A., Poloczanska, E., Pörtner, H.-O., Revi, A., Roberts, D. C., Roy, J., Ruane, A. C., Skea, J., Shukla, P. R., Slade, R., Slangen, A., Sokona, Y., Sörensson,
520 A. A., Tignor, M., Van Vuuren, D., Wei, Y.-M., Winkler, H., Zhai, P., Zommers, Z., Hourcade, J.-C., Johnson, F. X., Pachauri, S., Simpson, N. P., Singh, C., Thomas, A., Totin, E., Arias, P., Bustamante, M., Elgizouli, I., Flato, G., Howden, M., Méndez-Vallejo, C., Pereira, J. J., Pichs-Madruga, R., Rose, S. K., Saheb, Y., Sánchez Rodríguez, R., Ürge Vorsatz, D., Xiao, C., Yassaa, N., Alegría, A., Armour, K., Bednar-Friedl, B., Blok, K., Cissé, G., Dentener, F., Eriksen, S., Fischer, E., Garner, G., Guivarch, C., Haasnoot, M., Hansen, G., Hauser,

M., Hawkins, E., Hermans, T., Kopp, R., Leprince-Ringuet, N., Lewis, J., Ley, D., Ludden, C., Niamir, L., Nicholls, Z., Some, S., Szopa,
S., Trewin, B., Van Der Wijst, K.-I., Winter, G., Witting, M., Birt, A., Ha, M., Romero, J., Kim, J., Haites, E. F., Jung, Y., Stavins, R.,
Birt, A., Ha, M., Orendain, D. J. A., Ignon, L., Park, S., Park, Y., Reisinger, A., Cammaramo, D., Fischlin, A., Fuglestvedt, J. S., Hansen,
G., Ludden, C., Masson-Delmotte, V., Matthews, J. R., Mintenbeck, K., Pirani, A., Poloczanska, E., Leprince-Ringuet, N., and Péan, C.:
IPCC, 2023: Climate Change 2023: Synthesis Report. Contribution of Working Groups I, II and III to the Sixth Assessment Report of the
Intergovernmental Panel on Climate Change [Core Writing Team, H. Lee and J. Romero (eds.)]. IPCC, Geneva, Switzerland., Tech. rep.,
Intergovernmental Panel on Climate Change (IPCC), https://doi.org/10.59327/IPCC/AR6-9789291691647, edition: First, 2023.

Chapin, F. S., Sturm, M., Serreze, M. C., McFadden, J. P., Key, J. R., Lloyd, A. H., McGuire, A. D., Rupp, T. S., Lynch, A. H., Schimel,
J. P., Beringer, J., Chapman, W. L., Epstein, H. E., Euskirchen, E. S., Hinzman, L. D., Jia, G., Ping, C.-L., Tape, K. D., Thomp-
son, C. D. C., Walker, D. A., and Welker, J. M.: Role of Land-Surface Changes in Arctic Summer Warming, Science, 310, 657–660,
https://doi.org/10.1126/science.1117368, 2005.

Crameri, F., Shephard, G. E., and Heron, P. J.: The misuse of colour in science communication, Nature Communications, 11, 5444,
https://doi.org/10.1038/s41467-020-19160-7, 2020.

Curtis, P. G., Slay, C. M., Harris, N. L., Tyukavina, A., and Hansen, M. C.: Classifying drivers of global forest loss, Science, 361, 1108–1111,
https://doi.org/10.1126/science.aau3445, 2018.

Edwards, M. E., Brubaker, L. B., Lozhkin, A. V., and Anderson, P. M.: Structurally novel biomes: A response to past warming in Beringia,
Ecology, 86, 1696–1703, https://doi.org/10.1890/03-0787, 2005.

FAO and IIASA: Harmonized World Soil Database version 2.0, FAO; International Institute for Applied Systems Analysis (IIASA);,
https://doi.org/10.4060/cc3823en, 2023.

Field, C. B., ed.: Managing the risks of extreme events and disasters to advance climate change adaption: special report of the Intergovern-
mental Panel on Climate Change, Cambridge University Press, New York, NY, oCLC: ocn796030880, 2012.

Gerten, D., Schaphoff, S., Haberlandt, U., Lucht, W., and Sitch, S.: Terrestrial vegetation and water balance—hydrological evaluation of a
dynamic global vegetation model, Journal of Hydrology, 286, 249–270, https://doi.org/10.1016/j.jhydrol.2003.09.029, 2004.

Gregor, K., Knoke, T., Krause, A., Reyer, C. P. O., Lindeskog, M., Papastefanou, P., Smith, B., Lansø, A., and Rammig,
A.: Trade-Offs for Climate-Smart Forestry in Europe Under Uncertain Future Climate, Earth's Future, 10, e2022EF002 796,
https://doi.org/10.1029/2022EF002796, 2022.

Gustafson, A., Miller, P. A., Björk, R. G., Olin, S., and Smith, B.: Nitrogen restricts future sub-arctic treeline advance in an individual-based
dynamic vegetation model, Biogeosciences, 18, 6329–6347, https://doi.org/10.5194/bg-18-6329-2021, 2021.

Hansen, W. D., Braziunas, K. H., Rammer, W., Seidl, R., and Turner, M. G.: It takes a few to tango: changing climate and fire regimes can
cause regeneration failure of two subalpine conifers, Ecology, 99, 966–977, https://doi.org/10.1002/ecy.2181, 2018.

Hansen, W. D., Fitzsimmons, R., Olnes, J., and Williams, A. P.: An alternate vegetation type proves resilient and persists for decades following
forest conversion in the North American boreal biome, Journal of Ecology, 109, 85–98, https://doi.org/10.1111/1365-2745.13446, 2021.

Haxeltine, A. and Prentice, I. C.: BIOME3: An equilibrium terrestrial biosphere model based on ecophysiological constraints, resource
availability and competition among plant functional types, Global Biogeochemical Cycles, 10, 693–709, 1996.

Hijmans, R. J.: terra: Spatial data analysis, manual, https://CRAN.R-project.org/package=terra, 2023.

Hollinger, D. Y., Ollinger, S. V., Richardson, A. D., Meyers, T. P., Dail, D. B., Martin, M. E., Scott, N. A., Arkebauer, T. J., Baldocchi, D. D.,
Clark, K. L., Curtis, P. S., Davis, K. J., Desai, A. R., Dragoni, D., Goulden, M. L., Gu, L., Katul, G. G., Pallardy, S. G., Paw U, K. T.,

Schmid, H. P., Stoy, P. C., Suyker, A. E., and Verma, S. B.: Albedo estimates for land surface models and support for a new paradigm based on foliage nitrogen concentration, Global Change Biology, 16, 696–710, https://doi.org/10.1111/j.1365-2486.2009.02028.x, 2010.

Ilisson, T. and Chen, H. Y. H.: The direct regeneration hypothesis in northern forests, Journal of Vegetation Science, 20, 735–744, https://doi.org/10.1111/j.1654-1103.2009.01066.x, 2009.

565 Johnstone, J. F., Hollingsworth, T. N., Chapin, F. S., and Mack, M. C.: Changes in fire regime break the legacy lock on successional trajectories in Alaskan boreal forest, Global Change Biology, 16, 1281–1295, https://doi.org/10.1111/j.1365-2486.2009.02051.x, 2010.

Johnstone, J. F., Allen, C. D., Franklin, J. F., Frelich, L. E., Harvey, B. J., Higuera, P. E., Mack, M. C., Meentemeyer, R. K., Metz, M. R., Perry, G. L., Schoennagel, T., and Turner, M. G.: Changing disturbance regimes, ecological memory, and forest resilience, Frontiers in Ecology and the Environment, 14, 369–378, https://doi.org/10.1002/fee.1311, 2016.

570 Ju, W., Chen, J. M., Black, T. A., Barr, A. G., and McCaughey, H.: Spatially simulating changes of soil water content and their effects on carbon sequestration in Canada's forests and wetlands, Tellus B, 62, https://doi.org/10.3402/tellusb.v62i3.16521, 2010.

Kiljunen, N.: Creating value through advanced silvicultural services, Dissertationes Forestales, 2006, https://doi.org/10.14214/df.17, 2006.

Kim, J. E., Wang, J. A., Li, Y., Czimczik, C. I., and Randerson, J. T.: Wildfire-induced increases in photosynthesis in boreal forest ecosystems of North America, Global Change Biology, 30, e17 151, https://doi.org/10.1111/gcb.17151, 2024.

575 Krasting, J. P., Broccoli, A. J., Dixon, K. W., and Lanzante, J. R.: Future Changes in Northern Hemisphere Snowfall, Journal of Climate, 26, 7813–7828, https://doi.org/10.1175/JCLI-D-12-00832.1, 2013.

Krause, A., Haverd, V., Poulter, B., Anthoni, P., Quesada, B., Rammig, A., and Arneth, A.: Multimodel Analysis of Future Land Use and Climate Change Impacts on Ecosystem Functioning, Earth's Future, 7, 833–851, https://doi.org/10.1029/2018EF001123, 2019.

Lange, S. and Büchner, M.: ISIMIP3b bias-adjusted atmospheric climate input data, https://doi.org/10.48364/ISIMIP.842396.1, 2021.

580 Liu, Z., Ballantyne, A. P., and Cooper, L. A.: Increases in Land Surface Temperature in Response to Fire in Siberian Boreal Forests and Their Attribution to Biophysical Processes, Geophysical Research Letters, 45, 6485–6494, https://doi.org/10.1029/2018GL078283, 2018.

Liu, Z., Ballantyne, A. P., and Cooper, L. A.: Biophysical feedback of global forest fires on surface temperature, Nature Communications, 10, 214, https://doi.org/10.1038/s41467-018-08237-z, 2019.

Mack, M. C., Walker, X. J., Johnstone, J. F., Alexander, H. D., Melvin, A. M., Jean, M., and Miller, S. N.: Carbon loss from boreal forest 585 wildfires offset by increased dominance of deciduous trees, Science, 372, 280–283, https://doi.org/10.1126/science.abf3903, 2021.

Malhi, Y., Baldocchi, D. D., and Jarvis, P. G.: The carbon balance of tropical, temperate and boreal forests, Plant, Cell and Environment, 22, 715–740, https://doi.org/10.1046/j.1365-3040.1999.00453.x, 1999.

Massicotte, P. and South, A.: rnaturalearth: World map data from natural earth, manual, https://CRAN.R-project.org/package=rnaturalearth, 2023.

590 McCrystall, M. R., Stroeve, J., Serreze, M., Forbes, B. C., and Screen, J. A.: New climate models reveal faster and larger increases in Arctic precipitation than previously projected, Nature Communications, 12, 6765, https://doi.org/10.1038/s41467-021-27031-y, 2021.

McDowell, N. G., Allen, C. D., Anderson-Teixeira, K., Aukema, B. H., Bond-Lamberty, B., Chini, L., Clark, J. S., Dietze, M., Grossiord, C., Hanbury-Brown, A., Hurtt, G. C., Jackson, R. B., Johnson, D. J., Kueppers, L., Lichstein, J. W., Ogle, K., Poulter, B., Pugh, T. A. M., Seidl, R., Turner, M. G., Uriarte, M., Walker, A. P., and Xu, C.: Pervasive shifts in forest dynamics in a changing world, Science, 368, 595 eaaz9463, https://doi.org/10.1126/science.aaz9463, 2020.

Mekonnen, Z. A., Riley, W. J., Randerson, J. T., Grant, R. F., and Rogers, B. M.: Expansion of high-latitude deciduous forests driven by interactions between climate warming and fire, Nature Plants, 5, 952–958, https://doi.org/10.1038/s41477-019-0495-8, 2019.

Meyer, B. F., Darela-Filho, J., Gu, Q., Gregor, K., Krause, A., Papastefanou, P., Buras, A., Hesse, B., Asuk, S. A., Liu, D., Grams, T. E. E., Zang, C. S., and Rammig, A.: Leaf conductance, isohydric strategy, and Ϙ50 shape drought responses of European tree species in a dynamic vegetation model, https://doi.org/10.5194/egusphere-egu24-8421, 2024.

Miller, P. A. and Smith, B.: Modelling Tundra Vegetation Response to Recent Arctic Warming, AMBIO, 41, 281–291, https://doi.org/10.1007/s13280-012-0306-1, 2012.

Mitchell, S. J.: Wind as a natural disturbance agent in forests: a synthesis, Forestry, 86, 147–157, https://doi.org/10.1093/forestry/cps058, 2013.

Neigh, C., Nelson, R., Ranson, K., Margolis, H., Montesano, P., Sun, G., Kharuk, V., Naesset, E., Wulder, M., and Anderson, H.: LiDAR-based Biomass Estimates, Boreal Forest Biome, Eurasia, 2005-2006, p. 1113.356022 MB, https://doi.org/10.3334/ORNLDAAC/1278, artwork Size: 1113.356022 MB Publisher: ORNL Distributed Active Archive Center, 2015.

Neigh, C. S., Nelson, R. F., Ranson, K. J., Margolis, H. A., Montesano, P. M., Sun, G., Kharuk, V., Næsset, E., Wulder, M. A., and Andersen, H.-E.: Taking stock of circumboreal forest carbon with ground measurements, airborne and spaceborne LiDAR, Remote Sensing of Environment, 137, 274–287, https://doi.org/10.1016/j.rse.2013.06.019, 2013.

Nord, J., Anthoni, P., Gregor, K., Gustafson, A., Hantson, S., Lindeskog, M., Meyer, B., Miller, P., Nieradzik, L., Olin, S., Papaste-fanou, P., Smith, B., Tang, J., Wårlind, D., and And Past LPJ-GUESS Contributors.: LPJ-GUESS Release v4.1.1 model code, https://doi.org/10.5281/ZENODO.8065737, 2021.

Olson, D. M., Dinerstein, E., Wikramanayake, E. D., Burgess, N. D., Powell, G. V. N., Underwood, E. C., D'amico, J. A., Itoua, I., Strand, H. E., Morrison, J. C., Loucks, C. J., Allnutt, T. F., Ricketts, T. H., Kura, Y., Lamoreux, J. F., Wettengel, W. W., Hedao, P., and Kassem, K. R.: Terrestrial Ecoregions of the World: A New Map of Life on Earth, BioScience, 51, 933, https://doi.org/10.1641/0006-3568(2001)051[0933:TEOTWA]2.0.CO;2, 2001.

Pan, Y., Birdsey, R., Fang, J., Houghton, R., Kauppi, P., Kurz, W., Phillips, O., Shvidenko, A., Lewis, S., Canadell, J., Ciais, P., Jackson, R., Pacala, S., McGuire, A., Piao, S., Rautiainen, A., Sitch, S., and Hayes, D.: A Large and Persistent Carbon Sink in the World's Forests, Science (New York, N.Y.), 333, 988–93, https://doi.org/10.1126/science.1201609, 2011.

Papastefanou, P., Zang, C. S., Pugh, T. A. M., Liu, D., Grams, T. E. E., Hickler, T., and Rammig, A.: A Dynamic Model for Strategies and Dynamics of Plant Water-Potential Regulation Under Drought Conditions, Frontiers in Plant Science, 11, 373, https://doi.org/10.3389/fpls.2020.00373, 2020.

Papastefanou, P., Pugh, T., Buras, A., Eckes-Shephard, A., Fleischer, K., Grams, T., Gregor, K., Hickler, T., Krause, A., Lapola, D., Liu, D., Zang, C., and Rammig, A.: Diverging simulated effects of future drought stress on the Amazon rainforest , https://doi.org/10.5194/egusphere-egu22-12669, 2022.

Pebesma, E.: Simple Features for R: Standardized Support for Spatial Vector Data, The R Journal, 10, 439, https://doi.org/10.32614/RJ-2018-009, 2018.

Pebesma, E. and Bivand, R.: Spatial Data Science: With Applications in R, Chapman and Hall/CRC, New York, 1 edn., https://doi.org/10.1201/9780429459016, 2023.

Pedersen, T. L. and Crameri, F.: scico: Colour palettes based on the scientific colour-maps, manual, https://CRAN.R-project.org/package=scico, 2022.

Peros, M. C., Gajewski, K., and Viau, A. E.: Continental-scale tree population response to rapid climate change, competition and disturbance, Global Ecology and Biogeography, 17, 658–669, https://doi.org/10.1111/j.1466-8238.2008.00406.x, 2008.

635   Pfadenhauer, J. S. and Klötzli, F. A.: Global Vegetation: Fundamentals, Ecology and Distribution, Springer International Publishing, Cham,
       https://doi.org/10.1007/978-3-030-49860-3, 2020.

       Potapov, P., Hansen, M. C., Laestadius, L., Turubanova, S., Yaroshenko, A., Thies, C., Smith, W., Zhuravleva, I., Komarova, A., Minnemeyer,
       S., and Esipova, E.: The last frontiers of wilderness: Tracking loss of intact forest landscapes from 2000 to 2013, Science Advances, 3,
       e1600 821, https://doi.org/10.1126/sciadv.1600821, 2017.

640   Potter, S., Solvik, K., Erb, A., Goetz, S. J., Johnstone, J. F., Mack, M. C., Randerson, J. T., Román, M. O., Schaaf, C. L., Turetsky, M. R.,
       Veraverbeke, S., Walker, X. J., Wang, Z., Massey, R., and Rogers, B. M.: Climate change decreases the cooling effect from postfire albedo
       in boreal North America, Global Change Biology, 26, 1592–1607, https://doi.org/10.1111/gcb.14888, 2020.

       Pugh, T. A. M., Jones, C. D., Huntingford, C., Burton, C., Arneth, A., Brovkin, V., Ciais, P., Lomas, M., Robertson, E., Piao,
       S. L., and Sitch, S.: A Large Committed Long-Term Sink of Carbon due to Vegetation Dynamics, Earth's Future, 6, 1413–1432,
645   https://doi.org/10.1029/2018EF000935, 2018.

       Pugh, T. A. M., Arneth, A., Kautz, M., Poulter, B., and Smith, B.: Important role of forest disturbances in the global biomass turnover and
       carbon sinks, Nature Geoscience, 12, 730–735, https://doi.org/10.1038/s41561-019-0427-2, 2019a.

       Pugh, T. A. M., Lindeskog, M., Smith, B., Poulter, B., Arneth, A., Haverd, V., and Calle, L.: Role of forest regrowth in global carbon sink
       dynamics, Proceedings of the National Academy of Sciences, 116, 4382–4387, https://doi.org/10.1073/pnas.1810512116, 2019b.

650   R Core Team: R: A language and environment for statistical computing, manual, R Foundation for Statistical Computing, Vienna, Austria,
       https://www.R-project.org/, 2022.

       Rahmstorf, S. and Coumou, D.: Increase of extreme events in a warming world, Proceedings of the National Academy of Sciences, 108,
       17 905–17 909, https://doi.org/10.1073/pnas.1101766108, 2011.

       Rees, W. G., Hofgaard, A., Boudreau, S., Cairns, D. M., Harper, K., Mamet, S., Mathisen, I., Swirad, Z., and Tutubalina, O.: Is subarctic
655   forest advance able to keep pace with climate change?, Global Change Biology, 26, 3965–3977, https://doi.org/10.1111/gcb.15113, 2020.

       Reichstein, M., Bahn, M., Ciais, P., Frank, D., Mahecha, M. D., Seneviratne, S. I., Zscheischler, J., Beer, C., Buchmann, N., Frank, D. C.,
       Papale, D., Rammig, A., Smith, P., Thonicke, K., van der Velde, M., Vicca, S., Walz, A., and Wattenbach, M.: Climate extremes and the
       carbon cycle, Nature, 500, 287–295, https://doi.org/10.1038/nature12350, 2013.

       Rogers, B. M., Randerson, J. T., and Bonan, G. B.: High-latitude cooling associated with landscape changes from North American boreal
660   forest fires, Biogeosciences, 10, 699–718, https://doi.org/10.5194/bg-10-699-2013, 2013.

       Seidl, R., Thom, D., Kautz, M., Martin-Benito, D., Peltoniemi, M., Vacchiano, G., Wild, J., Ascoli, D., Petr, M., Honkaniemi, J., Lexer, M. J.,
       Trotsiuk, V., Mairota, P., Svoboda, M., Fabrika, M., Nagel, T. A., and Reyer, C. P. O.: Forest disturbances under climate change, Nature
       Climate Change, 7, 395–402, https://doi.org/10.1038/nclimate3303, 2017.

       Sitch, S., Smith, B., Prentice, I. C., Arneth, A., Bondeau, A., Cramer, W., Kaplan, J. O., Levis, S., Lucht, W., Sykes, M. T., Thonicke, K.,
665   and Venevsky, S.: Evaluation of ecosystem dynamics, plant geography and terrestrial carbon cycling in the LPJ dynamic global vegetation
       model: LPJ Dynami global vegetation model, Global Change Biology, 9, 161–185, https://doi.org/10.1046/j.1365-2486.2003.00569.x,
       2003.

       Smith, B., Prentice, I. C., and Sykes, M. T.: Representation of vegetation dynamics in the modelling of terrestrial ecosystems: comparing two
       contrasting approaches within European climate space: Vegetation dynamics in ecosystem models, Global Ecology and Biogeography, 10,
670   621–637, https://doi.org/10.1046/j.1466-822X.2001.t01-1-00256.x, 2001.

Smith, B., Wårlind, D., Arneth, A., Hickler, T., Leadley, P., Siltberg, J., and Zaehle, S.: Implications of incorporating N cycling and N limitations on primary production in an individual-based dynamic vegetation model, Biogeosciences, 11, 2027–2054, https://doi.org/10.5194/bg-11-2027-2014, 2014.

Sulla-Menashe, D., Woodcock, C. E., and Friedl, M. A.: Canadian boreal forest greening and browning trends: an analysis of biogeographic patterns and the relative roles of disturbance versus climate drivers, Environmental Research Letters, 13, 014 007, https://doi.org/10.1088/1748-9326/aa9b88, 2018.

Swann, A. L., Fung, I. Y., Levis, S., Bonan, G. B., and Doney, S. C.: Changes in Arctic vegetation amplify high-latitude warming through the greenhouse effect, Proceedings of the National Academy of Sciences, 107, 1295–1300, https://doi.org/10.1073/pnas.0913846107, 2010.

Tian, H., Yang, J., Lu, C., Xu, R., Canadell, J. G., Jackson, R. B., Arneth, A., Chang, J., Chen, G., Ciais, P., Gerber, S., Ito, A., Huang, Y., Joos, F., Lienert, S., Messina, P., Olin, S., Pan, S., Peng, C., Saikawa, E., Thompson, R. L., Vuichard, N., Winiwarter, W., Zaehle, S., Zhang, B., Zhang, K., and Zhu, Q.: The Global N2O Model Intercomparison Project, Bulletin of the American Meteorological Society, 99, 1231–1251, https://doi.org/10.1175/BAMS-D-17-0212.1, 2018.

Turner, M. G., Braziunas, K. H., Hansen, W. D., and Harvey, B. J.: Short-interval severe fire erodes the resilience of subalpine lodgepole pine forests, Proceedings of the National Academy of Sciences, 116, 11 319–11 328, https://doi.org/10.1073/pnas.1902841116, 2019.

Vaughan, D. and Dancho, M.: furrr: Apply mapping functions in parallel using futures, manual, https://CRAN.R-project.org/package=furrr, 2022.

Verbruggen, W., Schurgers, G., Meunier, F., Verbeeck, H., and Horion, S.: Simulated Tree-Grass Competition in Drylands Is Modulated by CO_2 Fertilization, Earth's Future, 12, e2023EF004 096, https://doi.org/10.1029/2023EF004096, 2024.

Wang, J. A. and Friedl, M. A.: The role of land cover change in Arctic-Boreal greening and browning trends, Environmental Research Letters, 14, 125 007, https://doi.org/10.1088/1748-9326/ab5429, 2019.

Wang, J. A., Sulla-Menashe, D., Woodcock, C. E., Sonnentag, O., Keeling, R. F., and Friedl, M. A.: Extensive land cover change across Arctic–Boreal Northwestern North America from disturbance and climate forcing, Global Change Biology, 26, 807–822, https://doi.org/10.1111/gcb.14804, 2020.

Wang, T., Zhang, H., Zhao, J., Guo, X., Xiong, T., and Wu, R.: Shifting Contribution of Climatic Constraints on Evapotranspiration in the Boreal Forest, Earth's Future, 9, e2021EF002 104, https://doi.org/10.1029/2021EF002104, 2021.

Wang, Z. and Zeng, X.: Evaluation of Snow Albedo in Land Models for Weather and Climate Studies, Journal of Applied Meteorology and Climatology, 49, 363–380, https://doi.org/10.1175/2009JAMC2134.1, 2010.

Warlind, D., Smith, B., Hickler, T., and Arneth, A.: Nitrogen feedbacks increase future terrestrial ecosystem carbon uptake in an individual-based dynamic vegetation model, Biogeosciences, 11, https://doi.org/10.5194/bg-11-6131-2014, 2014.

Warszawski, L., Friend, A., Ostberg, S., Frieler, K., Lucht, W., Schaphoff, S., Beerling, D., Cadule, P., Ciais, P., Clark, D. B., Kahana, R., Ito, A., Keribin, R., Kleidon, A., Lomas, M., Nishina, K., Pavlick, R., Rademacher, T. T., Buechner, M., Piontek, F., Schewe, J., Serdeczny, O., and Schellnhuber, H. J.: A multi-model analysis of risk of ecosystem shifts under climate change, Environmental Research Letters, 8, 044 018, https://doi.org/10.1088/1748-9326/8/4/044018, 2013.

Wickham, H.: ggplot2: Elegant Graphics for Data Analysis, Use R!, Springer International Publishing : Imprint: Springer, Cham, 2nd ed. 2016 edn., https://doi.org/10.1007/978-3-319-24277-4, 2016.

Wickham, H., Averick, M., Bryan, J., Chang, W., McGowan, L., François, R., Grolemund, G., Hayes, A., Henry, L., Hester, J., Kuhn, M., Pedersen, T., Miller, E., Bache, S., Müller, K., Ooms, J., Robinson, D., Seidel, D., Spinu, V., Takahashi, K., Vaughan, D., Wilke, C., Woo, K., and Yutani, H.: Welcome to the Tidyverse, Journal of Open Source Software, 4, 1686, https://doi.org/10.21105/joss.01686, 2019.

Wilke, C. O.: cowplot: Streamlined plot theme and plot annotations for 'ggplot2', manual, https://CRAN.R-project.org/package=cowplot, 2020.

Wolf, A., Callaghan, T. V., and Larson, K.: Future changes in vegetation and ecosystem function of the Barents Region, Climatic Change, 87, 51–73, https://doi.org/10.1007/s10584-007-9342-4, 2008.

Zani, D., Lischke, H., and Lehsten, V.: Climate and dispersal limitation drive tree species range shifts in post-glacial Europe: results from dynamic simulations, Frontiers in Ecology and Evolution, 11, 1321 104, https://doi.org/10.3389/fevo.2023.1321104, 2023.

Zhang, W., Miller, P. A., Smith, B., Wania, R., Koenigk, T., and Döscher, R.: Tundra shrubification and tree-line advance amplify arctic climate warming: results from an individual-based dynamic vegetation model, Environmental Research Letters, 8, 034 023, https://doi.org/10.1088/1748-9326/8/3/034023, 2013.

Zhang, W., Miller, P. A., Jansson, C., Samuelsson, P., Mao, J., and Smith, B.: Self-Amplifying Feedbacks Accelerate Greening and Warming of the Arctic, Geophysical Research Letters, 45, 7102–7111, https://doi.org/10.1029/2018GL077830, 2018.

Zhang, W., Döscher, R., Koenigk, T., Miller, P., Jansson, C., Samuelsson, P., Wu, M., and Smith, B.: The Interplay of Recent Vegetation and Sea Ice Dynamics—Results From a Regional Earth System Model Over the Arctic, Geophysical Research Letters, 47, https://doi.org/10.1029/2019GL085982, 2020.

Table A1. Overview over used PFTs

PFT	Full name	Example species
		Trees
BNE	Boreal needleleaf evergreen	*Picea abies* (L.) H.Karst.
BINE	Boreal shade-intolerant needleleaf evergreen	*Pinus sylvestris* L.
BNS	Boreal needleleaf summergreen	*Larix sibirica* Ledeb.
TeNE	Temperate needleleaf summergreen	
IBS	Shade-intolerant broadleaf summergreen	*Betula pubescens* Ehrh.,
		Populus tremula L.
TeBS	Temperate broadleaf summergreen	*Tilia cordata* Mill.,
		Ulmus glabra Huds.
		Shrubs
HSE	High shrub evergreen	*Juniperus communis* L.,
		Pinus pumila (Parl.) Regel
HSS	High shrub summergreen	*Salix* spp., *Betula nana* L.
LSE	Low shrub evergreen	*Vaccinium vitis-idaea* L.,
		Ledum palustre L.
LSS	Low shrub summergreen	*Vaccinium myrtillus* L , *Salix glauca* L.
EPDS	Prostrate dwarf shrub evergreen	*Vaccinium oxycoccus* L.
SPDS	Prostrate dwarf shrub summergreen	*Salix arctica* Pall.
		Non-woody PFTs
GRT	Graminoid and forb Tundra	Artemisia, Kobresia, Brassicaceae
CLM	Cushion forb, lichen and moss Tundra	Saxifragacea, Caryophyllaceae
C3G	Temperate C3 grasses	Gramineae

Appendix A: Methods

Appendix B: Results

Table A2. Overview over relevant PFT-related parameters

PFT	Leaf	Pheno	Shade	$t^E_{t,c,min}$	$t^E_{t,c,max}$	$t^E_{t,w,min}$	$GDD5^E_{min,i}$	$t^S_{t,c,min}$	L_i
BNE	NL	EG	tolerant	-30	-1	5	500	-31	500
BINE	NL	EG	intolerant	-30	-1	5	500	- 31	500
BNS	NL	SG	intolerant	-1000	-2	-1000	-1000	350	300
TeNE	NL	EG	intolerant	-2	10	5	2000	2	300
IBS	BL	SG	intolerant	-30	7	-1000	350	-30	300
TeBS	BL	SG	tolerant	-13	6	5	1100	-14	400
HSE	NL	EG	intolerant	-16	5	-	300	-32.5	100
HSS	BL	SG	intolerant	-32.5	5	-	300	-32.5	100
LSE	NL	EG	tolerant	-	5	-	100	-	25
LSS	BL	SG	tolerant	-	5	-	100	-	25
EPDS	NL	EG	tolerant	5	-	-	-	0	100
SPDS	BL	SG	tolerant	5	-	-	-	0	100
GRT	-			-	-	-	-	-	
CLM	-						0		
C3G	BL	-	-	-1000	-1000	-1000	-1000	1000	-

Table B1. Average Vegetation composition at the end of the spinup period (spatial and yearly mean across the years 1850 - 1880). Factorial simulations are restarted from this state.

PFT	AGC in kg/m^2	FPC in m^2/m^2	AGC in %	FPC in %
Needleleaf evergreen	2.8 ± 0.033	0.34 ± 0.079	80 ± 0.251	59 ± 0.997
Needleleaf summergreen	0.13 ± 0.013	0.01 ± 0.001	4 ± 0.273	2 ± 0.188
Pioneering broadleaf	0.53 ± 0.009	0.03 ± 0.001	10 ± 0.083	5 ± 0.184
Temperate broadleaf	$0.01 \pm 1e\text{-}04$	$0 \pm 1e\text{-}05$	0 ± 0.001	0 ± 0.002
Temperate needleleaf	0 ± 0	0 ± 0	0 ± 0	0 ± 0
Tundra	0.12 ± 0.004	0.19 ± 0.01	6 ± 0.352	34 ± 1.27
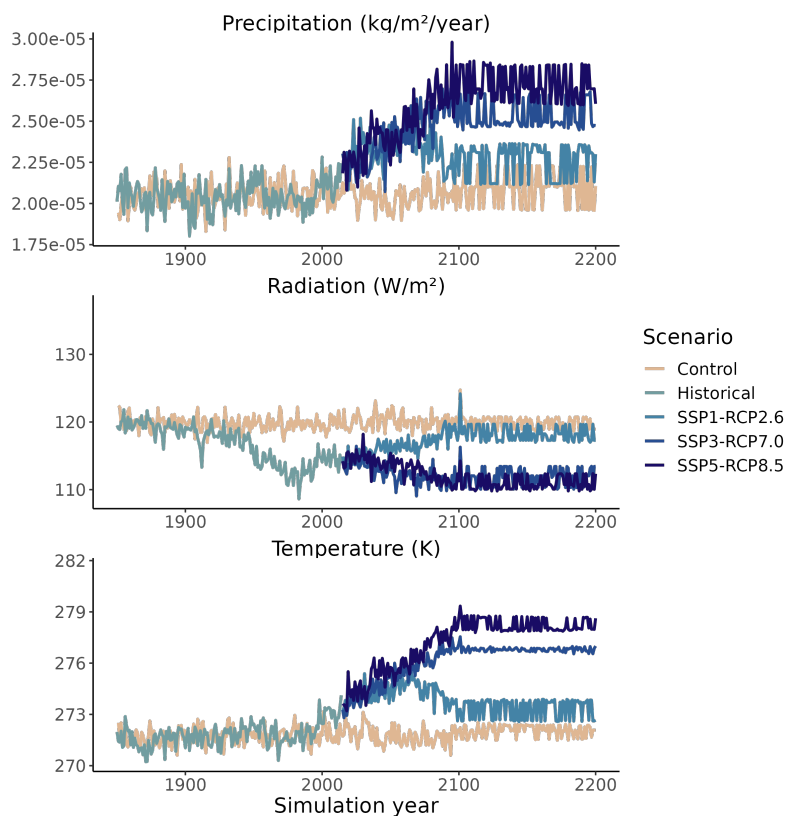
Figure A1. Climate data used to force the simulations. Note that model runs continue until 2500, further recycling data of the years 2095 - 2100.
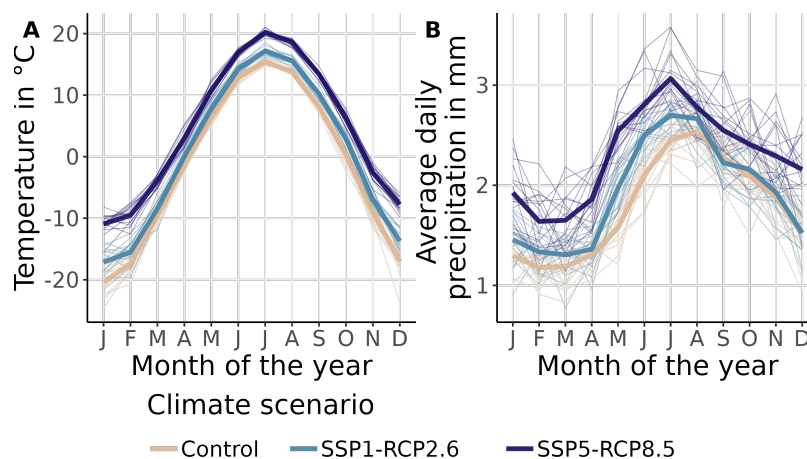
Figure B1. End of century seasonal temperature (**A**) and precipitation (**B**). Thick lines indicate mean over 2070 - 2100, thin lines individual years.
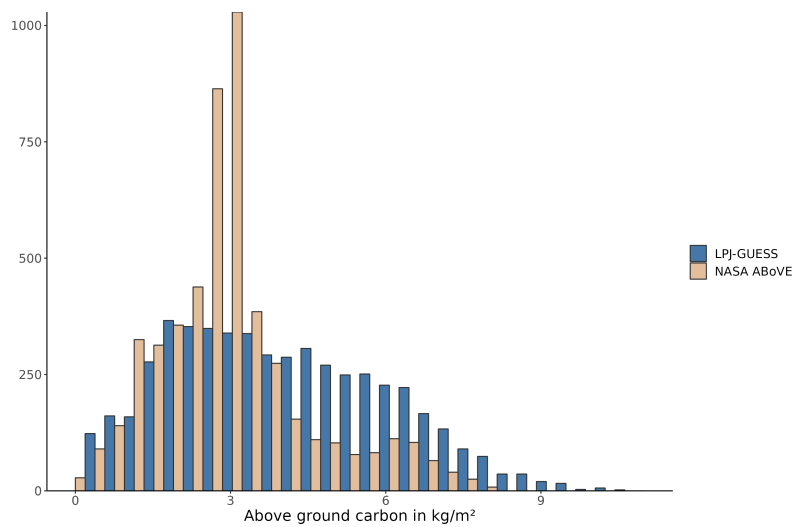
Figure B2. Comparing aboveground carbon (AGC) simulated by LPJ-GUESS with remotely-sensed AGC from NASA's AboVE mission. Both datasets show the year 2005 across the spatial domain.
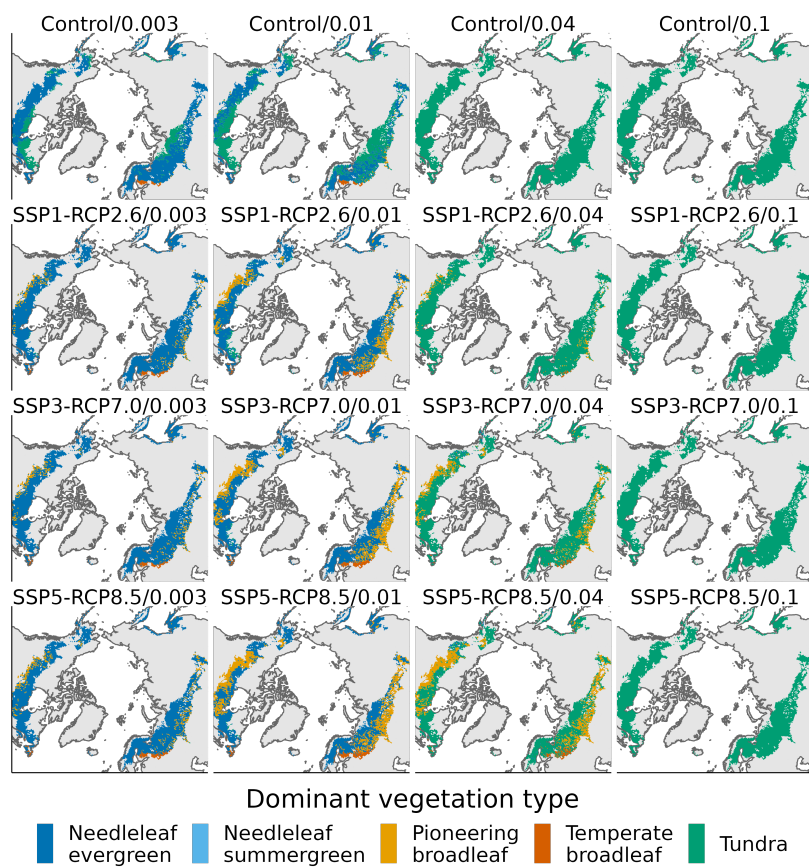
Figure B3. End-of-century dominant vegetation type for all configurations. Rows show a shift in climate, and columns a shift in disturbance regime.
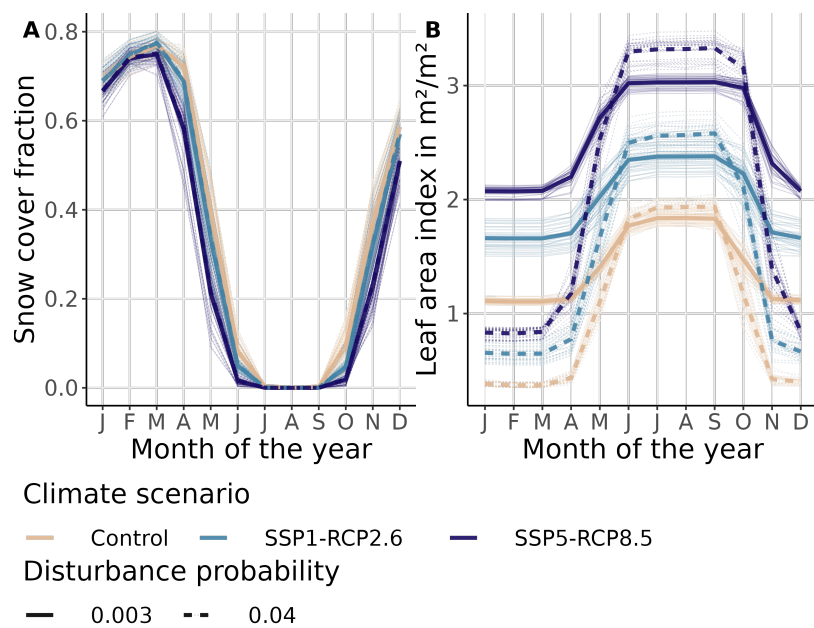
Figure B4. End of century seasonal curves of snow cover fraction (**A**) and total LAI (**B**). Thick lines indicate mean over 2070 - 2100, thin lines individual years.
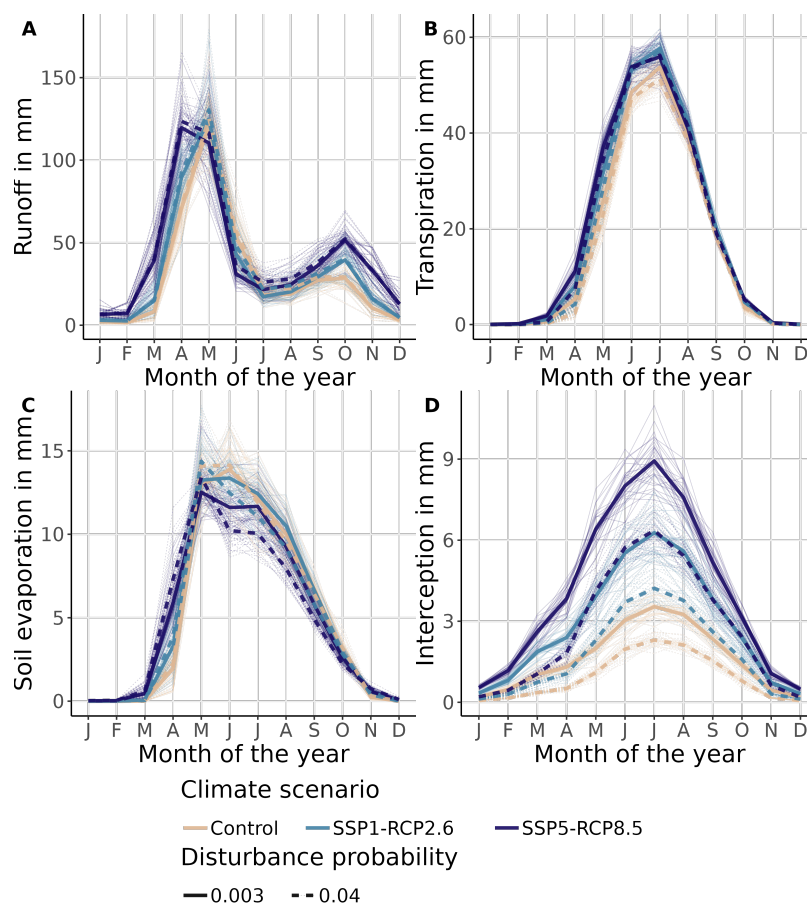
Figure B5. End of century seasonal curves for surface runoff (**A**), plant transpiration (**B**), soil evaporation (**C**) and leaf interception and evaporation (**D**). Evapotranspiration is the sum of **B**, **C** and **D**. Thick lines indicate mean over 2070 - 2100, thin lines individual years. Note the different y-Axis ranges of the individual panels.